Cell

Cyclic CMP and cyclic UMP mediate bacterial immunity against phages

Graphical abstract

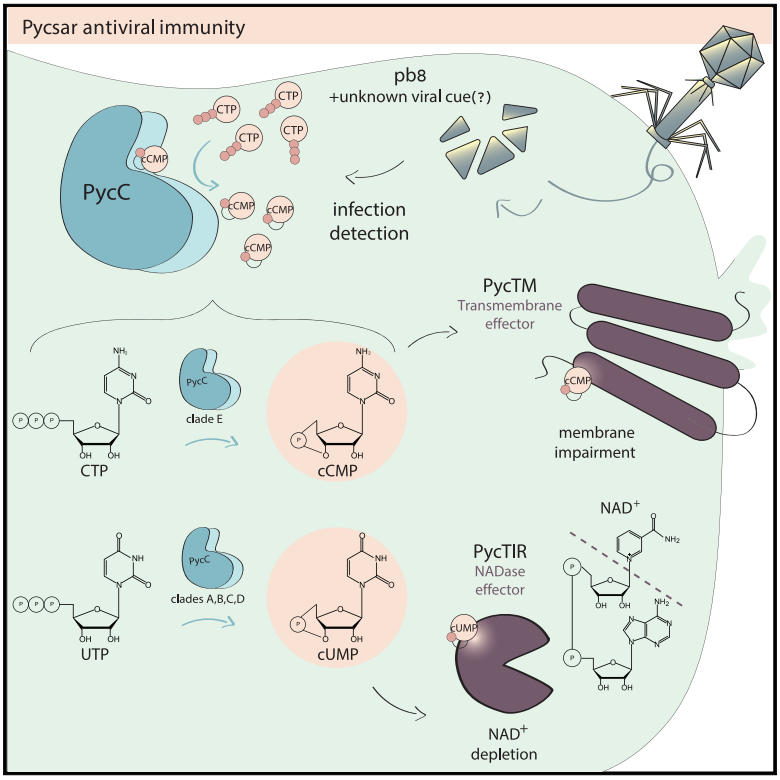

Highlights

- cCMP and cUMP are secondary messengers in a bacterial immune system called Pycsar
- cCMP and cUMP are produced following phage infection and activate immune effectors
- Structure of a uridylate cyclase explains the mechanism of pyrimidine selectivity
- Defense systems encoding pyrimidine cyclases are widespread in prokaryotes

Authors

Nitzan Tal, Benjamin R. Morehouse, Adi Millman, ..., Gil Amitai, Philip J. Kranzusch, Rotem Sorek

Correspondence

philip_kranzusch@dfci.harvard.edu (P.J.K.), rotem.sorek@weizmann.ac.il (R.S.)

In brief

The cyclic pyrimidines cCMP and cUMP serve as second messengers to activate antiviral immunity in bacteria.

Tal et al., 2021, Cell *184*, 1–12
November 11, 2021
https://doi.org/10.1016/j.cell.2021.09.031

CellPress

Please cite this article in press as: Tal et al., Cyclic CMP and cyclic UMP mediate bacterial immunity against phages, Cell (2021), https://doi.org/10.1016/j.cell.2021.09.031

Cell

CellPress

Article

Cyclic CMP and cyclic UMP mediate bacterial immunity against phages

Nitzan Tal,[1,7] Benjamin R. Morehouse,[2,3,7] Adi Millman,[1] Avigail Stokar-Avihail,[1] Carmel Avraham,[1] Taya Fedorenko,[1] Erez Yirmiya,[1] Ehud Herbst,[1] Alexander Brandis,[4] Tevie Mehlman,[4] Yaara Oppenheimer-Shaanan,[1] Alexander F.A. Keszei,[5] Sichen Shao,[5] Gil Amitai,[1] Philip J. Kranzusch,[2,3,6,*] and Rotem Sorek[1,8,*]

[1]Department of Molecular Genetics, Weizmann Institute of Science, Rehovot 7610001, Israel
[2]Department of Microbiology, Harvard Medical School, Boston, MA 02115, USA
[3]Department of Cancer Immunology and Virology, Dana-Farber Cancer Institute, Boston, MA 02115, USA
[4]Life Sciences Core Facilities, Weizmann Institute of Science, Rehovot 7670001, Israel
[5]Department of Cell Biology, Harvard Medical School, Boston, MA 02115, USA
[6]Parker Institute for Cancer Immunotherapy at Dana-Farber Cancer Institute, Boston, MA 02115, USA
[7]These authors contributed equally
[8]Lead contact
*Correspondence: philip_kranzusch@dfci.harvard.edu (P.J.K.), rotem.sorek@weizmann.ac.il (R.S.)
https://doi.org/10.1016/j.cell.2021.09.031

SUMMARY

The cyclic pyrimidines 3′,5′-cyclic cytidine monophosphate (cCMP) and 3′,5′-cyclic uridine monophosphate (cUMP) have been reported in multiple organisms and cell types. As opposed to the cyclic nucleotides 3′,5′-cyclic adenosine monophosphate (cAMP) and 3′,5′-cyclic guanosine monophosphate (cGMP), which are second messenger molecules with well-established regulatory roles across all domains of life, the biological role of cyclic pyrimidines has remained unclear. Here we report that cCMP and cUMP are second messengers functioning in bacterial immunity against viruses. We discovered a family of bacterial pyrimidine cyclase enzymes that specifically synthesize cCMP and cUMP following phage infection and demonstrate that these molecules activate immune effectors that execute an antiviral response. A crystal structure of a uridylate cyclase enzyme from this family explains the molecular mechanism of selectivity for pyrimidines as cyclization substrates. Defense systems encoding pyrimidine cyclases, denoted here Pycsar (pyrimidine cyclase system for antiphage resistance), are widespread in prokaryotes. Our results assign clear biological function to cCMP and cUMP as immunity signaling molecules in bacteria.

INTRODUCTION

Cyclic nucleotide monophosphates are ubiquitous signaling molecules that function as second messengers in all domains of life. Cyclic adenosine monophosphate (cAMP) is the most common cyclic nucleotide with widespread roles in prokaryotic and eukaryotic signaling. In bacteria, cAMP signaling controls gene expression and is essential for growth and adaptation to glucose starvation (Green et al., 2014; Pastan and Perlman, 1970). In eukaryotic cells, cAMP activates protein kinase signaling, allowing cells to respond to external stimuli. Human and animal cells additionally use 3′,5′-cyclic guanosine monophosphate (cGMP) as a second messenger, which regulates vasodilation through relaxation of smooth muscle tissue and also functions in the vertebrate visual system (Lincoln, 1989; Stryer, 1986). Growing evidence suggests that cGMP also serves as a second messenger in bacteria (Linder, 2010; Rauch et al., 2008; Ryu et al., 2015).

cAMP and cGMP are generated by adenylate and guanylate cyclase enzymes that convert ATP and guanosine triphosphate (GTP) into cyclized products. cAMP/cGMP cyclases comprise distinct enzyme classes, with class III adenylate/guanylate cyclases exhibiting the most widespread organismal distribution. Class III cyclase enzymes function as obligate dimers (Khannpnavar et al., 2020). The cyclase active site is composed of residues contributed from each enzyme protomer that together coordinate a divalent metal cation-dependent reaction and catalyze synthesis of cAMP and cGMP in response to upstream stimuli (Steegborn, 2014).

In contrast to the well-established functions of cAMP and cGMP, the existence and possible functional importance of cyclic pyrimidine nucleotides, 3′,5′-cyclic cytosine monophosphate (cCMP) and 3′,5′-cyclic uridine monophosphate (cUMP), remain controversial (Gaion and Krishna, 1979; Seifert, 2015). The presence of cCMP in mammalian tissues was reported more than three decades ago (Newton et al., 1984), and advancements in mass spectrometry methods have enabled detection of cCMP and cUMP in cells from multiple animals (Bähre et al., 2014, 2015). Although cCMP/cUMP have been hypothesized to be involved in diverse processes, including development and apoptotic cell death (Seifert, 2017), to date it is not known whether cCMP/cUMP have specific biological roles or

Please cite this article in press as: Tal et al., Cyclic CMP and cyclic UMP mediate bacterial immunity against phages, Cell (2021), https://doi.org/10.1016/j.cell.2021.09.031

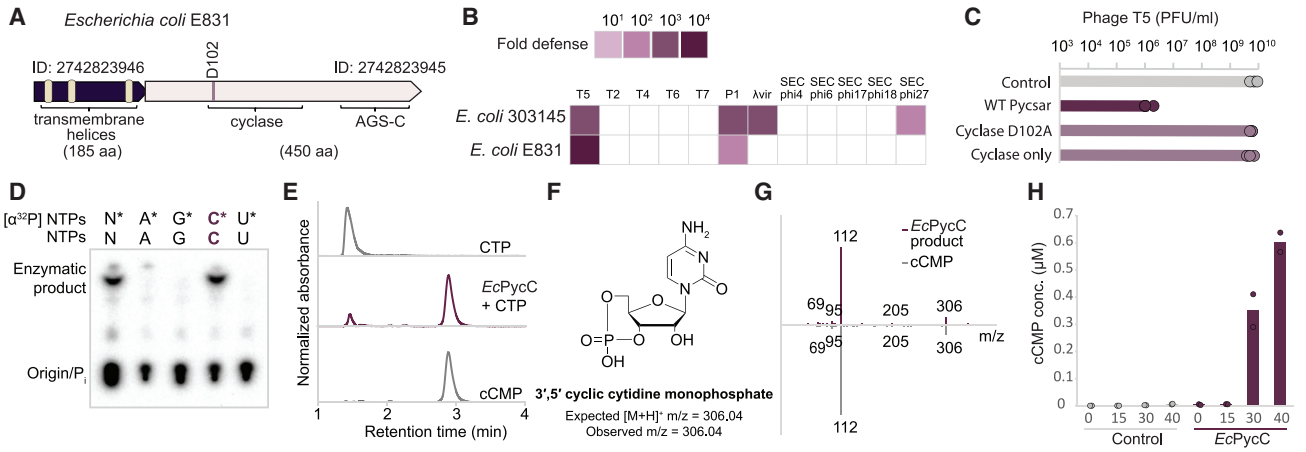

Figure 1. The Pycsar defense system encodes a cytidylate cyclase

(A) A two-gene system encoding a protein with a nucleotide cyclase domain and a protein with transmembrane (TM) helices from *Escherichia coli* E831. The gene IDs in the IMG database (Chen et al., 2019) are shown above the genes.

(B) Pycsar systems defend against phages. Systems from two *E. coli* strains were cloned together with the native promoter regions and transformed into *E. coli* MG1655. Fold defense was measured using serial dilution plaque assays, comparing the efficiency of plating of phages on the Pycsar-containing strain with that of the control strain that lacks the system. Data represent an average of three replicates (see detailed data in Figure S1B).

(C) Mutation in the active site of the predicted cyclase domain (D102A, predicted to abolish metal binding) or deletion of the TM domain gene abolishes the defensive activity of Pycsar from *E. coli* E831. Data represent plaque-forming units (PFUs) per milliliter of T5 phages infecting control cells, cells expressing the WT Pycsar from *E. coli* E831, and cells expressing mutated Pycsar. Shown is the average of three replicates, with individual data points overlaid.

(D) Thin-layer chromatography analysis of nucleotide second messenger synthesis by the *E. coli* E831 cyclase (*Ec*PycC). N, all four NTPs; P_i, inorganic phosphate. Data are representative of 3 independent experiments.

(E) HPLC analysis of chemical standards compared with the product of *Ec*PycC.

(F) Chemical structure of 3′,5′-cyclic cytidine monophosphate (cCMP).

(G) MS/MS fragmentation spectra of a cCMP standard (bottom) and the cyclase product (top).

(H) Concentrations of cCMP in lysates extracted from *Ec*PycC-expressing cells or control GFP-expressing cells that were infected by T5 phage, as measured by LC-MS/MS with synthesized cCMP standard. The x axis represents minutes after infection, with zero representing non-infected cells. Cells were infected by phage T5 at an MOI of 2 at 37°C. *Ec*PycC expression was induced by 0.2% arabinose. Bar graphs represent the average of two biological replicates, with individual data points overlaid.

whether these molecules are by-products of weak, non-specific activity of adenylate and guanylate cyclases.

In this study, we report a family of bacterial pyrimidine cyclases that synthesize cCMP and cUMP as the primary products. By determining the crystal structure of a uridylate cyclase from this family, we identify a unique active-site configuration that explains selection of UTP as the primary substrate for cyclization. We further show that cCMP/cUMP cyclases function as part of a family of bacterial antiphage defense systems and that production of cyclic pyrimidine molecules is triggered specifically by phage infection. The cCMP and cUMP molecules then activate effector proteins that execute abortive infection through membrane impairment or depletion of cellular NAD^+. Our results show that cytidylate and uridylate cyclases are widespread in bacteria and archaea and establish a biological function of cyclic pyrimidines as second messengers mediating bacterial immunity.

RESULTS

A defense system that produces cCMP

We analyzed ~40,000 microbial genomes for uncharacterized genes potentially involved in antiphage defense and identified a family of genes with an annotated adenylate cyclase protein domain. Analysis of this gene family revealed 967 bacterial and archaeal genes with frequent genomic localization next to known defense systems such as CRISPR-Cas and restriction modification, a trait common to many phage resistance systems (Figure S1A; Table S1; STAR Methods; Doron et al., 2018). Because adenylate cyclase proteins have important housekeeping regulatory roles in all domains of life (Hanoune and Defer, 2001), we were intrigued by their possible roles in phage defense. The predicted cyclase genes are usually found in an operon together with an additional gene (Figure 1A), and we therefore cloned two such two-gene operons, one from *Escherichia coli* 303145 and the other from *E. coli* E831, into the laboratory *E. coli* strain MG1655. Challenging the transformed bacteria with a panel of 12 phages showed that both operons provided substantial defense against multiple phages (Figure 1B; Figure S1B). Mutation in the predicted active site of the cyclase domain abolished defense, suggesting that the nucleotide cyclase activity is essential for the defensive capacity of the system (Figure 1C). Expression of the cyclase gene alone did not protect from infection, indicating that the second gene in the operon is also essential for defense against phages (Figure 1C).

We next expressed and purified the predicted adenylate cyclase from *E. coli* E831 and analyzed its enzymatic activity by thin-layer chromatography. Incubation of the purified protein

Please cite this article in press as: Tal et al., Cyclic CMP and cyclic UMP mediate bacterial immunity against phages, Cell (2021), https://doi.org/10.1016/j.cell.2021.09.031

with radiolabeled ATP resulted in no significant production of cAMP, counter to the hypothesized enzymatic activity that was predicted by homology-based protein annotation (Figure 1D). To test whether the protein uses other nucleotides as substrates, we incubated it with radiolabeled GTP, CTP, and UTP. Remarkably, the protein efficiently converted CTP into a new product that migrated as a single species (Figure 1D). Enzymatic activity was dependent on the presence of Mn^{2+} and occurred over a wide pH range from 7.0–9.5 (Figures S2A and S2B). Liquid chromatography-tandem mass spectrometry (LC-MS/MS) analysis compared with a chemically synthesized standard showed that the product of the enzymatic activity is 3′,5′-cyclic cytidine monophosphate (cCMP) (Figures 1E–1G; Figure S2C). These results demonstrate that this *E. coli* defensive gene codes for a cytidylate cyclase, an enzyme that, to our knowledge, has been hypothesized previously (Seifert, 2015) but never identified. We therefore named the defense system Pycsar (pyrimidine cyclase system for antiphage resistance) and denoted the cyclase domain-containing gene *pycC*.

To confirm that this enzyme also synthesizes cCMP *in vivo*, we used LC-MS/MS to examine production of cCMP in *E. coli* MG1655 cells expressing the PycC cyclase protein from *E. coli* E831. We could not detect cCMP above the background level in lysates derived from exponentially growing cells (Figure 1H). However, in lysates derived from phage-infected cells, we detected substantial levels of cCMP (Figure 1H). The cCMP molecules begun accumulating between 15 and 30 min after initial infection by phage T5 but did not accumulate in infected control cells lacking the cyclase, indicating that cCMP is indeed produced by the cyclase and suggesting that cCMP production *in vivo* is stimulated by phage infection (Figure 1H).

A family of pyrimidine cyclases that mediate phage resistance

We next constructed a phylogenetic tree using multiple sequence alignment of the cyclase domain in the 967 bacterial and archaeal *pycC* genes. The tree topology showed that these proteins form five major clades, with the cCMP cyclases verified in this study found in clade E (Figure 2A). Closely related sequences from the same clade were frequently derived from bacteria and archaea of diverse phyla, suggesting horizontal gene transfer between phylogenetically distant organisms. To examine the substrate specificity of enzymes in this family of nucleotide cyclase enzymes, we selected two protein representatives from each clade, expressed and purified them, and incubated them with radiolabeled nucleotides. Surprisingly, proteins from clades A–D did not use CTP as substrate but, rather, showed strong uridylate cyclase activities, converting UTP to cUMP (Figures 2B–2E; Figures S3A and S3B). We tested a Pycsar system from *Xanthomonas perforans*, encoding a PycC cyclase from clade B, and found that it provided defense against phage T7 (Figure 2F).

Some of the tested proteins, and specifically the ones from clade D, also showed minor guanylate cyclase activities (Figure 2B; Figure S3C) in addition to producing cUMP as the major product. Adenylate cyclase activities were very low in all tested proteins, suggesting strong selection against cAMP production that might interfere with cAMP-dependent cellular regulatory processes (Figure 2B; Figure S2C).

The domain organization of the pyrimidine cyclases varied between clades. In clades B, C, and D, the nucleotide cyclase domain was the only identifiable domain within the protein sequence, whereas clade E cyclases also contained an AGS-C domain, which has been found previously to be fused to signal-producing proteins in CBASS antiphage systems and hypothesized to serve as a phage recognition domain (Burroughs et al., 2015; Millman et al., 2020a). Structural prediction of the AGS-C domain suggests that it adopts an immunoglobulin-like fold (Figure S3D), supporting the hypothesis that it might be used in phage detection. Deletion of the AGS-C domain of *Ec*PycC rendered the system inactive against phages (Figure S3E). PycC proteins from clade A contained two consecutive nucleotide cyclase domains as opposed to single cyclase domains in other clades (Figure 2A).

Uridylate cyclase structure reveals the molecular basis for pyrimidine cyclization

To understand the molecular principles defining the substrate specificity of pyrimidine-specific cyclase enzymes, we determined a 1.5-Å crystal structure of a clade B uridylate cyclase from *Burkholderia cepacia* LK29 (*Bc*PycC) (Figure 3A; Table S1). The *Bc*PycC crystal structure reveals a two-fold symmetric homodimeric enzyme with three main α helices wrapped around a central anti-parallel β sheet. *Bc*PycC shares clear structural homology with class III adenylate and guanylate cyclase proteins conserved in prokaryotic and eukaryotic signaling systems (Steegborn, 2014). Unlike most class III enzymes, *Bc*PycC has an additional α helix (α7′) at the N terminus that makes contact with α helices 2 and 3 of the opposing protomer (Figure 3A).

Analysis of the *Bc*PycC active site reveals that each protomer in the homodimeric enzyme contains catalytic aspartate residues, D52 and D96, required for divalent metal ion coordination, and a conserved asparagine at position N172, predicted to contact the ribose ester oxygen (Figures 3B–3D; Figure S4A). Substitutions at either of these sites abolished cUMP synthesis (Figure 3E), supporting the theory that *Bc*PycC uses the same highly conserved catalytic mechanism shared by all class III cyclase enzymes (Linder, 2005; Tesmer et al., 1999). Using the structure of a mammalian class III adenylate cyclase in complex with an ATP analog as a guide (Tesmer et al., 1999), we modeled a UTP nucleotide into the *Bc*PycC active site to identify residues involved in pyrimidine selection (Figures 3B and 3C). Class III adenylate and guanylate cyclases control nucleobase selectivity through base-specific contacts with a pair of highly conserved lysine and aspartate residues (adenylate cyclases) or cysteine and glutamate residues (guanylate cyclases) (Linder, 2005; Steegborn, 2014). Notably, the *Bc*PycC nucleotide binding pocket lacks analogous side chains positioned for purine nucleotide selection. Instead, in *Bc*PycC residues, Y50, D94, and R97 protrude into the nucleotide binding pocket and sterically occlude the space required to coordinate ATP or GTP (Figure S4B). *Bc*PycC residues Y50 and R97 are conserved in cUMP synthases from clade B. Likewise, cCMP synthases (clade E), including *Ec*PycC, are predicted to contain F and R residues at similar structural positions, suggesting a role of these amino acids in PycC pyrimidine base selection (Figures S4C and

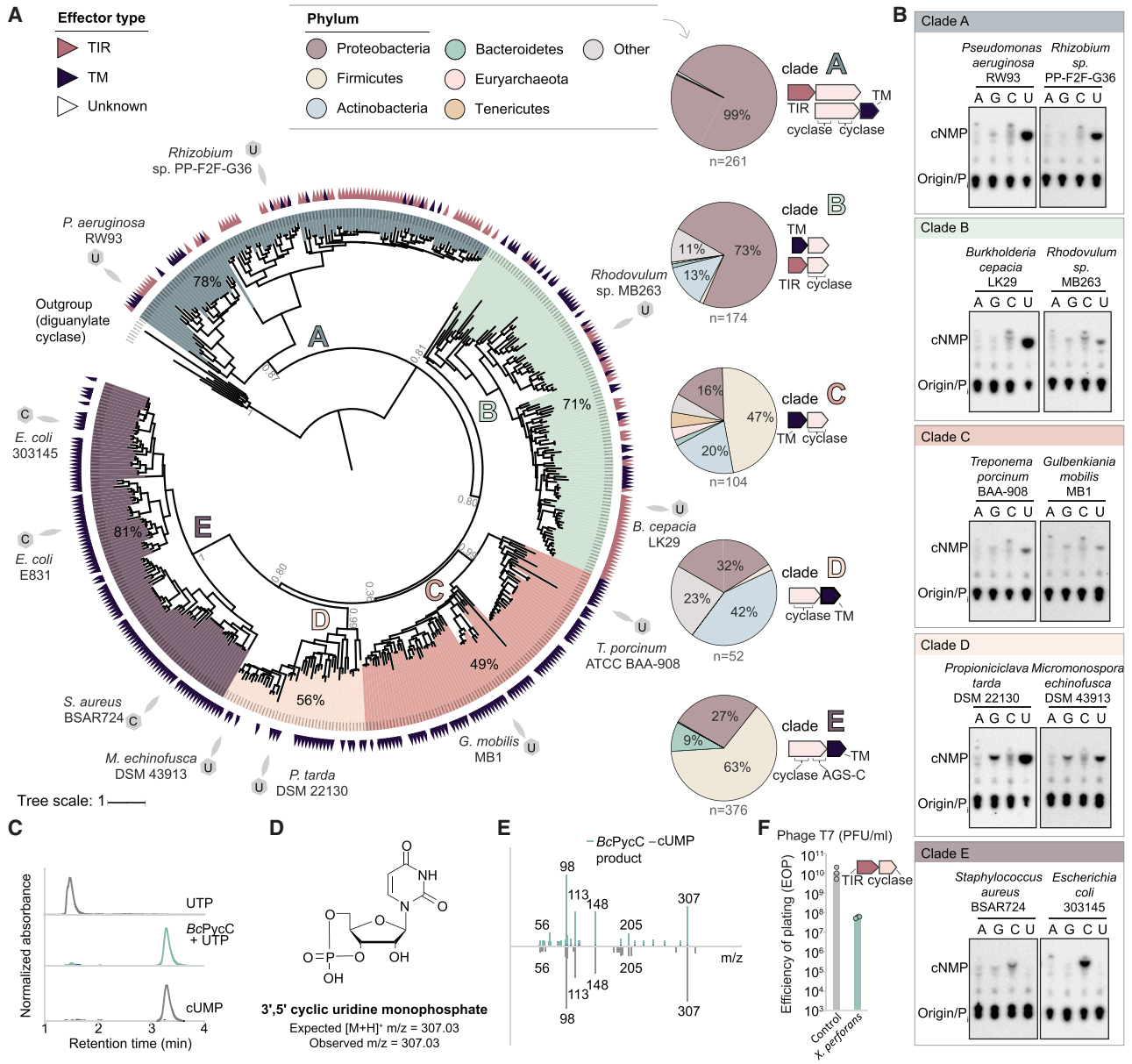

Figure 2. Diversity of pyrimidine cyclases in prokaryotic genomes

(A) Phylogenetic tree of proteins with pyrimidine cyclase domains. Only non-redundant sequences were used to build the tree (Table S1). The percentage of genes that are located near known defense genes is indicated for each clade. Bootstrap values are indicated for major clades. The outermost ring indicates the type of effector gene that is associated with the cyclase gene. Top left: color code for the effector types. Pie charts represent the phylum distribution of cyclase-containing prokaryotes in each of the clades on the tree. The common domain organization of the Pycsar system in each clade is presented to the right of the pie chart. Genes for which cyclase activity was demonstrated *in vitro* are marked by gray wedges, with U marking cUMP production and C marking cCMP.

(B) Thin-layer chromatography analysis of cyclase proteins from two representatives of each clade. Data are representative of 3 independent experiments.

(C) HPLC analysis of chemical standards compared with the enzymatic product of the *Bc*PycC cyclase.

(D) Chemical structure of 3′,5′-cyclic uridine monophosphate (cUMP).

(E) MS/MS fragmentation spectra of a cUMP standard (bottom) and the *Bc*PycC cyclase product (top).

(F) A Pycsar system from *Xanthomonas perforans* GEV1001, when cloned into *E. coli* MG1655, defends against phage T7. Data represent PFUs units per milliliter of T7 phages infecting control cells and system-expressing cells. Shown is the average of three replicates, with individual data points overlaid.

S4D). Using alanine scanning mutagenesis, we next tested substitutions to each *Bc*PycC and *Ec*PycC active site residue. *Bc*PycC and *Ec*PycC nucleobase pocket mutations reduced activity, but most of them did not completely abolish cCMP/cUMP synthesis *in vitro* (Figure 3E). *In vivo* experiments, however, showed that nucleobase pocket mutations abolished defense

Please cite this article in press as: Tal et al., Cyclic CMP and cyclic UMP mediate bacterial immunity against phages, Cell (2021), https://doi.org/10.1016/j.cell.2021.09.031

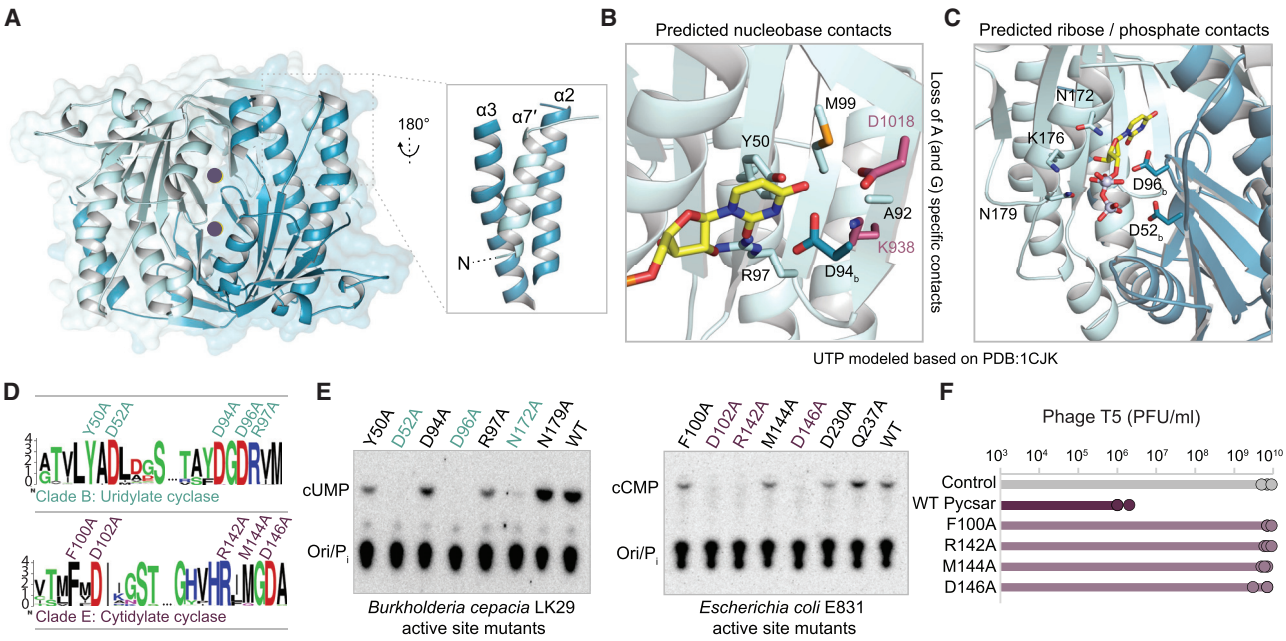

Figure 3. Structural and functional analyses of pyrimidine cyclases

(A) Crystal structure of a uridylate cyclase from *Burkholderia cepacia* LK29. Individual protomers of the homodimer are depicted in light and dark blue. Active site locations are denoted by purple circles.

(B) Magnified cutaway of the nucleotide binding pocket in the cUMP cyclase structure. UTP modeled into the apo protein active site highlights potential amino acid interactions ($_b$ denotes an opposing monomer). D1018 and K938 are residues essential for adenylate selectivity in mammalian adenylate cyclases and are modeled here from superposition of *Bc*PycC with a mammalian soluble adenylate cyclase (PDB: 1CJK).

(C) Magnified cutaway of predicted phosphate and ribose interactions in the cUMP cyclase structure.

(D) Conserved motifs in cUMP and cCMP cyclase of clade B and clade E, respectively. The residues mutated in *B. cepacia* LK29 and *E. coli* E831 PycC cyclases are indicated above.

(E) Thin-layer chromatography analysis of pyrimidine cyclase mutants of *Burkholderia cepacia* LK29 (left) and *Escherichia coli* E831 (right). Pi, inorganic phosphate; ori., origin. The mutations in the cyclase proteins are indicated above. Marked in colors are mutations that completely abolished cUMP/cCMP production.

(F) Plating efficiency of phage T5 on control cells, *E. coli* E831 Pycsar-expressing cells, and strains mutated in the cyclase protein. Data represent PFUs per milliliter, with the average of three replicates with individual data points overlaid.

in bacteria (Figure 3F). These results explain how Pycsar cyclases have evolved for pyrimidine specificity.

The structure of a *Pseudomonas aeruginosa* cyclase from clade A of the PycC phylogenetic tree has been determined previously, and it was observed that the protein lacks adenylate or guanylate cyclase activities (PDB: 6YII; Linder et al., 2020). We purified this *P. aeruginosa* protein (renamed here *Pa*PycC) and demonstrated that *Pa*PycC is an active uridylate cyclase (Figure 2B). Structural comparison of the clade A *Pa*PycC and the clade B *Bc*PycC shows that the α7′ helix we identified at the N terminus of *Bc*PycC is also present in the *Pa*PycC structure, suggesting that this helix may be a hallmark of PycC pyrimidine cyclases. Although *Bc*PycC comprised a homodimer, *Pa*PycC is encoded as a single chain with the two consecutive nucleotide cyclase domains folding into a pseudo-heterodimeric structure (Linder et al., 2020). In *Pa*PycC, the C-terminal cyclase domain contributes the metal binding residues, and the N-terminal cyclase domain presumably provides the binding pocket for nucleobase-selective residues (Linder et al., 2020). Such tandem domain configurations on a single protein chain are common in mammalian class III adenylate cyclase enzymes, although, in these enzymes, the architecture of the two domains is reversed compared with *Pa*PycC (Steegborn, 2014). A previous biochemical analysis of *Pa*PycC showed that it can bind ATP, as determined by isothermal titration calorimetry, and the *Pa*PycC structure was solved in complex with ATP (Linder et al., 2020). However, the configuration of ATP bound within *Pa*PycC has been shown to be incompatible with ATP hydrolysis or cAMP formation (Figure S4E; Linder et al., 2020). Analysis of the predicted UTP binding pocket within *Pa*PycC shows that many residues are conserved with *Bc*PycC, including the *Bc*PycC Y50 and R97 residues, predicted to sterically occlude purine bases (Figures S4E–S4G). These results further support the theory that the active-site architecture of PycC enzymes selectively prevents ATP/GTP use to specify pyrimidine nucleotide selection.

cCMP and cUMP activate effector genes that mediate abortive infection

Our results suggest that phage infection stimulates Pycsar cyclases to produce cCMP and cUMP. To understand the roles of these molecules in mediating the bacterial response to infection, we next analyzed the operons in which these cyclases are embedded. These operons typically contain at least one additional gene, which is essential for defense against phages

Please cite this article in press as: Tal et al., Cyclic CMP and cyclic UMP mediate bacterial immunity against phages, Cell (2021), https://doi.org/10.1016/j.cell.2021.09.031

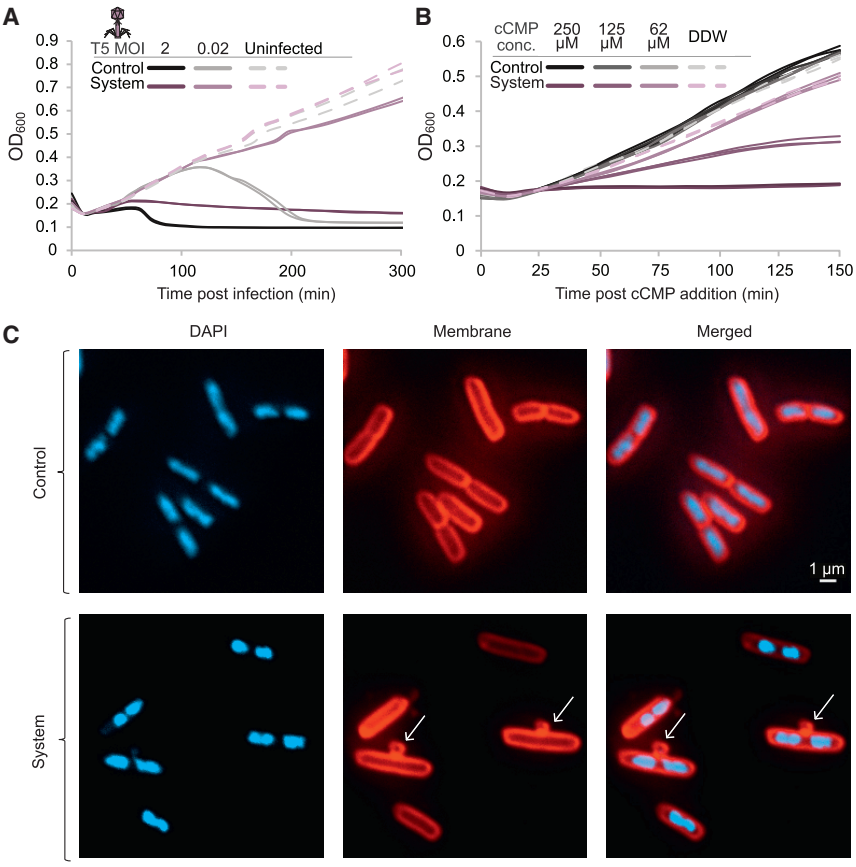

Figure 4. cCMP mediates abortive infection in Pycsar

(A) Growth curves of cells expressing the Pycsar system from *E. coli* E831 (purple) and control cells (black) with and without infection by phage T5 at a multiplicity of infection (MOI) of 2 or 0.02. Results of three experiments are presented as individual curves.

(B) Growth curves of Pycsar-expressing cells (purple) and control cells (black) with and without addition of various concentrations of cCMP to the medium or double-distilled water (DDW) control. Results of three experiments are presented as individual curves.

(C) Fluorescence microscopy images of *E. coli* MG1655 cells expressing the Pycsar system from *E. coli* E831 (bottom panel) or control cells lacking the system (top panel). Shown are DNA (blue) and membrane (red) stains. Images were captured 60 min after addition of 250 μM cCMP to the medium. Arrows point to abnormal membrane protrusions. Representative images from a single replicate of three independent replicates are shown.

(Figures 1 and 2). In some cases, the additional gene contains an N-terminal domain annotated as "cyclic nucleotide-binding domain" (pfam: PF00027), which is common in proteins that bind and are regulated by cyclic nucleotides such as cAMP and cGMP (Gomelsky and Galperin, 2013; Figure S5A; Table S1). This suggests that the second protein binds the cyclic nucleotide produced by the cyclase in response to phage infection and serves as the effector of the Pycsar system. In the majority of cases, the effector gene encodes an additional domain, either a domain with one to four transmembrane helices (57%) or a Toll/interleukin-1 receptor (TIR) domain (30%), and we denoted these effector genes *pycTM* and *pycTIR*, respectively (Figure 2A). Transmembrane helix domains and TIR domains are found frequently in bacterial defense systems such as CBASS (Cohen et al., 2019; Millman et al., 2020a; Morehouse et al., 2020) and retrons (Millman et al., 2020b), where, when activated, they are responsible for inflicting cell death or growth arrest before the phage is able to replicate, a process called abortive infection (Lopatina et al., 2020).

To test whether the systems that encode pyrimidine cyclases defend by triggering abortive infection, we performed infection experiments in liquid culture with cells encoding the Pycsar system from *E. coli* E831, which comprises a PycTM effector protein with three predicted transmembrane helices and a cytidylate cyclase (Figure 1). At a multiplicity of infection (MOI) of 0.02, where ~2% of bacteria are infected by the initial phage inoculum, the culture of wild-type cells collapsed because of phage propagation, whereas the culture of cells containing the Pycsar system survived (Figure 4A). Conversely, at an MOI of 2, where almost all bacteria are infected by the initial phage inoculum, the culture containing the Pycsar operon entered a state of growth stasis (Figure 4A). These results are consistent with a phenotype of abortive infection, where growth arrest of infected bacteria eliminates infected cells from the bacterial population and protects the culture from spread of the phage (Lopatina et al., 2020).

To directly determine whether the effector protein is activated by cCMP to impose a toxic effect on the cell, we incubated cells expressing the *E. coli* E831 Pycsar in medium supplemented with chemically synthesized cCMP. Although cCMP is a polar molecule that is not expected to efficiently diffuse through cell membranes, we reasoned that, at high enough concentrations in the growth medium, some cCMP molecules will be able to reach the interior of the cell and activate the effector. Indeed, Pycsar-expressing cells showed severe growth arrest in the presence of 250 μM cCMP (Figure 4B). cCMP did not cause growth arrest in control cells that did not express the defense system, suggesting that the toxicity is inflicted by the system following exposure to cCMP (Figure 4B). Addition of chemically synthesized cUMP to the growth medium did not cause toxicity, suggesting that the *E. coli* E831 PycTM effector is specific to the cCMP molecule produced by its cognate PycC cyclase (Figure S5B). Growth arrest was associated with the appearance of abnormal membrane protrusions in some of the cells, suggesting that the transmembrane-spanning effector exerts its toxicity by impairing membrane integrity, as suggested for transmembrane-spanning effectors of the CBASS (Millman et al., 2020a) and retron abortive infection defense systems (Millman et al., 2020b; Figure 4C).

Please cite this article in press as: Tal et al., Cyclic CMP and cyclic UMP mediate bacterial immunity against phages, Cell (2021), https://doi.org/10.1016/j.cell.2021.09.031

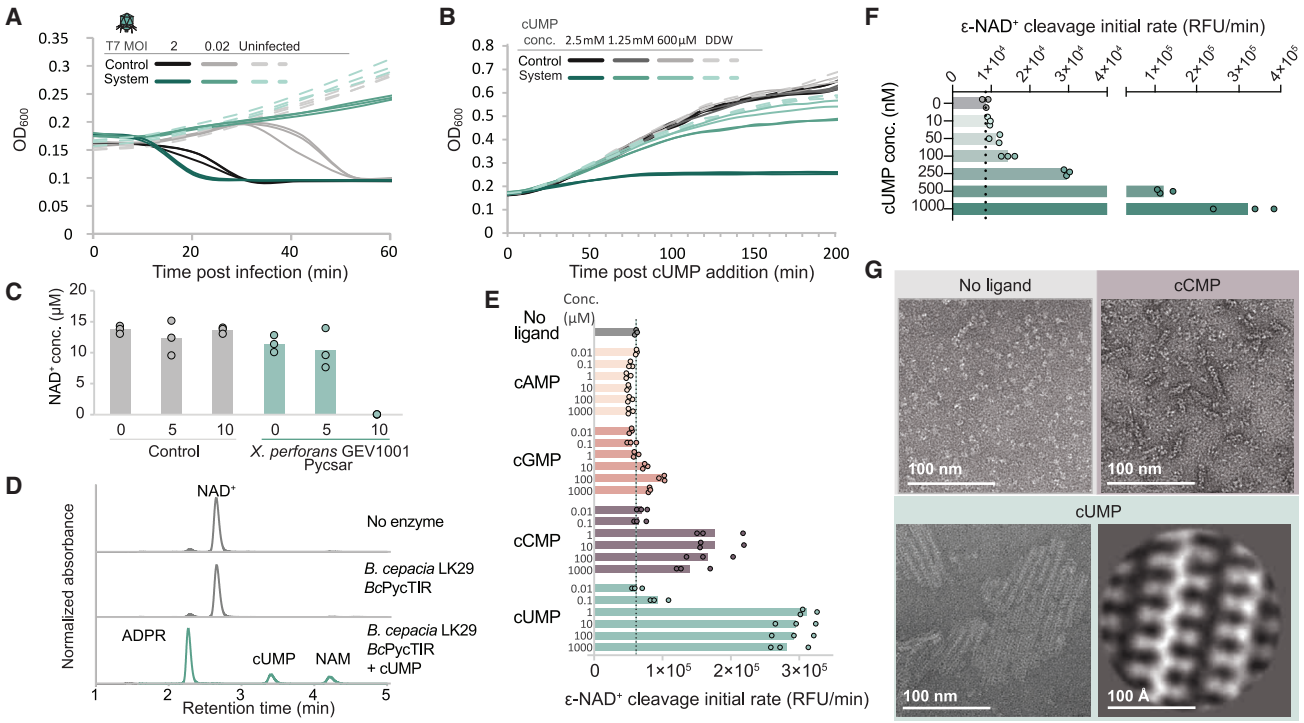

Figure 5. cUMP activates Pycsar TIR effectors that execute abortive infection

(A) Growth curves of cells expressing the cyclase-TIR Pycsar system from *Xanthomonas perforans* GEV1001 (green) and control cells (black) with and without infection by phage T7 at an MOI of 2 or 0.02. Results of three experiments are presented as individual curves.

(B) Growth curves of *Xp*Pycsar-expressing cells (green) and control cells (black) with and without addition of cUMP to the medium. Results of three experiments are presented as individual curves.

(C) Concentrations of NAD^+ in lysates extracted from *Xp*Pycsar-expressing cells and control cells, infected by phage T7, as measured by LC-MS/MS with synthesized NAD^+ standard. The x axis represents minutes after infection, with zero representing non-infected cells. Cells were infected by phage T7 at an MOI of 2 at 37°C. Bar graphs represent the average of three biological replicates, with individual data points overlaid.

(D) HPLC analysis of effector-mediated NAD^+ cleavage by *Bc*PycTIR. The TIR domain effector cleaves NAD^+ into the products ADP-ribose (ADPR) and nicotinamide (NAM), and the activity is strictly dependent on the presence of the cUMP molecule. cUMP was added at a concentration of 250 nM and incubated for 1 h with the TIR effector from *B. cepacia* LK29 at 500 nM in the presence of 500 µM NAD^+. Data are representative of 3 independent experiments.

(E) Analysis of NAD^+ cleavage activity of *Bc*PycTIR using the fluorescent substrate ε-NAD^+ at varying concentration of cNMPs. Data are the average of three biological replicates with individual data points overlaid.

(F) NAD^+ cleavage activity of *Bc*PycTIR in response to cUMP at a finer resolution of concentration span compared with (E).

(G) Electron microscopy analysis of *Bc*PycTIR filament formation in the presence of 50 µM cCMP or cUMP or without a ligand. The 2D class average of the effector when activated by cUMP is presented at the bottom right.

The second-most abundant effector gene in Pycsar systems, which encodes a TIR domain (*pycTIR*), is associated with uridylate cyclases (Figure 2). The cyclase-TIR Pycsar system from *X. perforans* also demonstrated an abortive infection phenotype in liquid culture infection experiments (Figure 5A), and addition of high-concentration cUMP to the medium resulted in growth arrest whereas addition of cCMP to the cells did not (Figure 5B; Figure S5C). TIR domain effectors in microbial defense systems are known to serve as NADases that deplete the cell of NAD^+ when they receive a signal indicative of phage infection, leading to abortive infection (Morehouse et al., 2020). Indeed, NAD^+ was completely depleted from cells expressing the *X. perforans* Pycsar during infection by phage T7 (Figure 5C). We purified the TIR domain effector protein from *Burkholderia cepacia* LK29 (*Bc*PycTIR), which is found in the same defense operon as the crystallized *BcPycC* uridylate cyclase (Figures 2 and 5). Incubation of *Bc*PycTIR with cUMP triggered robust NADase activity, as observed by high-performance LC (Figure 5D). *Bc*PycTIR activation generated the expected NAD^+ degradation products ADP-ribose and nicotinamide (Figure 5D). We next tested the cNMP-specificity of this TIR effector protein using a fluorescent NAD^+ analog. *Bc*PycTIR exhibited strong selectivity for cyclic pyrimidines, with ~50–100 nM cUMP sufficient for robust NADase activation (Figures 5E and 5F). Conversely, cAMP, even when added at millimolar concentrations, did not activate *Bc*PycTIR (Figure 5E).

Activation of TIR NADase domains is known to occur through protein oligomerization (Jiang et al., 2020; Morehouse et al., 2020; Sporny et al., 2019). To determine the mechanism of cNMP-mediated effector activation, we next used negative-stain electron microscopy to image *Bc*PycTIR in the presence of cUMP. Remarkably, *Bc*PycTIR recognition of cUMP resulted in

Please cite this article in press as: Tal et al., Cyclic CMP and cyclic UMP mediate bacterial immunity against phages, Cell (2021), https://doi.org/10.1016/j.cell.2021.09.031

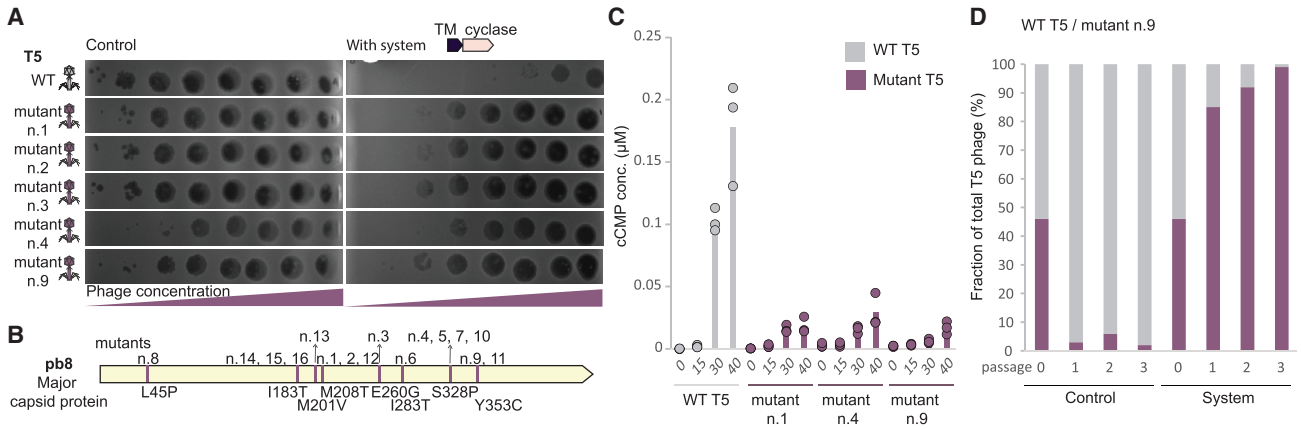

Figure 6. Phage escape from Pycsar-mediated defense

(A) Representative phage mutants capable of escaping defense by the Pycsar system of *E. coli* E831. Shown are 10-fold serial dilution plaque assays, comparing the plating efficiency of WT and mutant phages on *E. coli* MG1655 cells that contain the system and a control strain that lacks the system and contains an empty vector instead. Mutations of all escape mutant phages are detailed in Table S2.

(B) Positions of mutations within the T5 Pb8 protein.

(C) Concentrations of cCMP in cell lysates extracted from cells infected by WT or mutant T5 phages, as measured by LC-MS/MS with synthesized cCMP standard. The x axis represents minutes after infection, with zero representing non-infected cells. Cells were infected at an MOI of 2 at 37°C. Bar graphs represent the average of three biological replicates, with individual data points overlaid. *Ec*PycC expression was induced by 0.02% arabinose.

(D) A competition fitness assay between WT and mutant T5 phage on *Ec*Pycsar-expressing and control cells. The y axis represents the fraction of each strain of the total phage mixture based on sequenced DNA reads. The x axis represents the infection passage, with 0 representing the mixture prior to first passage. In each passage, phage lysate was taken and used for infection of a fresh bacterial culture.

formation of large, 100- to 300-nm, two-dimensional sheets (Figure 5G). 2D class averages revealed that the *Bc*PycTIR sheets are constructed from interlocking individual filaments resembling a zipper-like configuration. cCMP, a weak activator of *Bc*PycTIR NADase activity, induced formation of short flexible filaments (Figure 5G). These results explain how cyclic pyrimidine signaling drives *Bc*PycTIR NADase activation and further support the theory that protein oligomerization is a common mechanism controlling effector function in antiphage defense (Lowey et al., 2020; Morehouse et al., 2020).

Phages can evolve to escape Pycsar-mediated defense

To determine whether phages can evolve to evade Pycsar systems, we attempted to isolate phage mutants that could overcome the defense conferred by the *E. coli* E831 cytidylate cyclase and its cognate effector. We were able to isolate 17 such mutants of phage T5 that partially escaped defense and sequenced the full genome of each of these mutants. In almost all of these escapee phages (16 of 17), we identified a missense point mutation within the gene D20-21, encoding the pb8 protein, the major capsid protein precursor of T5 (Figures 6A and 6B; Table S2). Pb8 is the main component of the T5 head, forming an icosahedral capsid shell that contains 775 pb8 protomers (Huet et al., 2019). In all cases, the point mutations resulted in an amino acid substitution, and in most cases, the mutation in pb8 was the only mutation differing between the mutant and wild-type (WT) phage, indicating that single amino acid alterations in the T5 major capsid protein enable the phage to escape defense (Table S2).

We next measured production of cCMP in cells expressing the *Ec*PycC cyclase during infection by mutant phages. Mutant phages elicited substantially less cCMP production at 40 min following phage infection compared with WT T5 phages (Figure 6C). These results suggest that the cytidylate cyclase is activated less efficiently by the mutant phages, leading to reduced cCMP production and, hence, allowing phage escape from defense.

Overexpression of pb8 in cells expressing the Pycsar system did not elicit effector-mediated toxicity, suggesting that activation of the cyclase may necessitate another factor in addition to the pb8 capsid precursor (Figure S6A). We were also unable to demonstrate binding between pb8 and the cytidylate cyclase, and co-incubation of purified *Ec*PycC with pb8 did not increase its cyclase activity rate *in vitro* (Figures S6B–S6D). These results imply that the interaction between the two proteins is indirect or, again, necessitates a factor in addition to pb8.

To examine whether the escape mutations in pb8 confer a fitness cost to the phage, we performed competition assays between WT and mutant T5 strains. For this, we infected a liquid culture of bacteria with a mixture of WT and mutant T5 phages and measured the ratio between WT and mutant phages following several infection cycles (Figure 6D). As expected, the mutant phage rapidly took over the phage mixture when infecting cells expressing Pycsar because the system protects from the WT phage but not from the mutant (Figure 6D). However, when infecting cells not expressing the Pycsar system, the mutant phage was almost eliminated from the phage mixture after a single passage (Figure 6D). The results were replicated for other phage mutants (Figures S6E and S6F). These results suggest that mutations conferring resistance to Pycsar-mediated defense also result in a severe fitness cost to the phage and are

Please cite this article in press as: Tal et al., Cyclic CMP and cyclic UMP mediate bacterial immunity against phages, Cell (2021), https://doi.org/10.1016/j.cell.2021.09.031

thus expected to be selected against in natural settings in which the majority of bacterial hosts do not encode the defense system.

DISCUSSION

After decades of debate regarding whether cCMP and cUMP have distinct biological roles (Seifert, 2015, 2017; Seifert et al., 2011), our results show that these molecules are essential second messengers in Pycsar defense systems, establishing a function for cyclic pyrimidines in bacterial immunity. Our data show high specificity for cyclic pyrimidines in Pycsar systems. PycC cyclases have strong preference to produce cCMP or cUMP with almost no adenylate cyclase activity, and although PycTIR effectors are robustly activated by 50–100 nM of cUMP, they are not responsive to cAMP even at millimolar concentrations. It is likely that this strong substrate selectivity of Pycsar has evolved to prevent interference with house-keeping regulation by cAMP.

The enzymes of the PycC family reported here have been predicted to be involved in phage defense based on their close proximity to known defense genes, and in particular genes typically associated with CBASS systems (cap genes) (Millman et al., 2020a), leading to the prediction that they would produce immune signaling molecules. However, based on sequence annotation, these enzymes were incorrectly predicted to synthesize cAMP or cGMP derivatives. We show that cCMP and cUMP produced by PycC proteins in response to phage infection act as signaling molecules that mediate cell death. This discovery joins the recent identification of immune mechanisms such as type III CRISPR-Cas, CBASS, and Thoeris, all of which rely on production of a unique signaling compound that activates downstream effectors to prevent phage propagation in an infected cell (Cohen et al., 2019; Kazlauskiene et al., 2017; Ofir et al., 2021). These mechanistically diverse systems, utilizing a variety of signaling molecules and effectors, represent a conserved immunological principle where production of a second messenger mediates the immune response. Enzymatic production of the signaling molecule rapidly amplifies the signal upon phage recognition and presumably accelerates execution of the immune response (Lopatina et al., 2020).

cCMP and cUMP have been detected in human cells and implicated previously in early embryonic development (cCMP) (Chan, 1987) and promotion of apoptotic cell death (cUMP) (Beckert et al., 2014). Recent studies have demonstrated conserved immune functions for signaling molecules between bacteria and eukaryotes: cGMP-AMP (cGAMP) is produced by the cGAS-STING antiviral pathway in animals as well as by CBASS antiviral systems in bacteria (Bernheim and Sorek, 2020; Cohen et al., 2019; Morehouse et al., 2020; Whiteley et al., 2019), and TIR immune proteins generate similar signaling molecules in bacteria and plants (Ofir et al., 2021). It is therefore intriguing to speculate that cCMP and cUMP may function as immune signaling molecules in eukaryotes as well. We envision that our identification of the unique composition of the active site in PycC pyrimidine cyclases, which determines the strong specificity to CTP or UTP as substrates, may allow future discovery of pyrimidine cyclase enzymes in other organisms, including eukaryotes, and would ultimately extend our understanding on the biological roles of cCMP and cUMP.

Limitations of the study

It is important to understand how the Pycsar system senses phage replication. We found that *in vivo*, the Pycsar system produces cyclic nucleotides only in response to phage infection. However, purified PycC enzymes produce cyclic signaling molecules even without a phage-derived stimulus. One explanation for these findings is that recognition of phage replication *in vivo* results in PycC clustering and activation of cyclic nucleotide synthesis because of a sharp increase in local enzyme concentration. PycC activity *in vitro* in the absence of phage recognition could therefore be explained by the elevated concentration of highly purified protein. Alternatively, similar to sensors that function as guards in plant innate immunity pathways and detect pathogens indirectly (Dodds and Rathjen, 2010), PycC enzymes may be inhibited by a cellular co-factor *in vivo* that is depleted during phage replication. Finally, discovery of the Pycsar system provides an opportunity to explain how cyclase enzymes discriminate between purine and pyrimidine bases. Our analysis of the apo structure of *Bc*PycC reveals an active-site configuration associated with pyrimidine selection. Determining the structure of PycC in complex with pyrimidine nucleotide substrates and defining the mechanism of cCMP/cUMP recognition by downstream Pycsar receptors will be important goals for future studies.

STAR★METHODS

Detailed methods are provided in the online version of this paper and include the following:

- KEY RESOURCES TABLE
- RESOURCE AVAILABILITY
  - Lead contact
  - Materials availability
  - Data and code availability
- EXPERIMENTAL MODEL AND SUBJECT DETAILS
  - Bacterial strains and phages
- METHOD DETAILS
  - Detection of cNMP cyclase systems in defense islands
  - Plasmid and strain construction
  - Plaque assays
  - Infection in liquid culture
  - cCMP/cUMP supplementation assays
  - Cell lysate preparation
  - Quantification of nucleotides by HPLC-MS/MS
  - Mass spectrometry of *in vitro* reactions
  - Thermal denaturation assay
  - Isolation of mutant phages
  - Amplification of mutant phages
  - Sequencing and genome analysis of phage mutants
  - Microscopy of infected cells
  - Phylogenetic analysis
  - Fitness assay of mutant pb8 phages
  - Protein expression and purification
  - Crystallization and structure determination

- Thin-layer chromatography analysis of cyclic nucleotide products
- High-performance liquid chromatography analysis of enzymatic reactions
- Fluorescence plate reader analysis of NADase activity
- Negative stain electron microscopy and processing
- Pb8 binding assay

● QUANTIFICATION AND STATISTICAL ANALYSIS

SUPPLEMENTAL INFORMATION

Supplemental information can be found online at https://doi.org/10.1016/j.cell.2021.09.031.

ACKNOWLEDGMENTS

We thank the Sorek and Kranzusch laboratory members for comments on the manuscript and fruitful discussions and the Molecular Electron Microscopy Suite at Harvard Medical School. We thank Brianna Duncan-Lowey for assistance with predicting AGS-C homology to immunoglobulin folds. R.S. was supported in part by the European Research Council (ERC-CoG 681203), the Ernest and Bonnie Beutler Research Program of Excellence in Genomic Medicine, German Research Council (DFG) Priority Program SPP 2330 (SO 1611/2), the Minerva Foundation with funding from the Federal German Ministry for Education and Research, the Knell Family Center for Microbiology, the Yotam Project and the Weizmann Institute Sustainability and Energy Research (SAERI) initiative, and the Dr. Barry Sherman Institute for Medicinal Chemistry. P.J.K. was supported by grants from the Pew Biomedical Scholars Program, the Mark Foundation For Cancer Research, The Mathers Foundation, the Parker Institute for Cancer Immunotherapy, and a Burroughs Wellcome Fund PATH award. B.R.M. was supported as a Ruth L. Kirschstein NRSA Postdoctoral Fellow (NIH F32GM133063). A.M. was supported by a fellowship from the Ariane de Rothschild Women Doctoral Program and in part by the Israeli Council for Higher Education via the Weizmann Data Science Research Center and by a research grant from Madame Olga Klein-Astrachan. S.S. was supported by grants from the Vallee Scholars Program and a Packard fellowship.

AUTHOR CONTRIBUTIONS

N.T., B.R.M., P.J.K., and R.S. led the study and performed all analyses and experiments unless otherwise indicated. N.T. performed the genetic analyses and the *in vivo* experimental assays and analyzed the data. Structural and *in vitro* biochemical experiments were performed by B.R.M. A.M. and N.T. performed the computational analyses of systems prediction. A.S.-A. designed and executed the mutant phage isolation experiments and their analysis. C.A. assisted with plaque assays and DNA isolation of mutant phages. T.F. assisted with isolation of mutant phages and conducting plaque assays. E.Y. assisted with cyclase domain sequence analysis. E.H. designed the analytical pipeline for analysis of metabolomics data. G.A. assisted with sequence analysis and prediction of protein domain functions. A.B. and T.M. performed mass spectrometry and data analysis. Y.O.-S. performed the microscopy analysis. Electron microscopy experiments and analysis were conducted by A.F.A.K. and S.S. with assistance from B.R.M. The manuscript was written by N.T., B.R.M., P.J.K., and R.S. All authors contributed to editing the manuscript and support the conclusions.

DECLARATION OF INTERESTS

R.S. is a scientific cofounder and advisor of BiomX, Pantheon Bioscience, and Ecophage.

Received: June 30, 2021
Revised: August 23, 2021
Accepted: September 20, 2021
Published: October 12, 2021

REFERENCES

Altschul, S.F., Gish, W., Miller, W., Myers, E.W., and Lipman, D.J. (1990). Basic local alignment search tool. J. Mol. Biol. *215*, 403–410.

Bähre, H., Danker, K.Y., Stasch, J.P., Kaever, V., and Seifert, R. (2014). Nucleotidyl cyclase activity of soluble guanylyl cyclase in intact cells. Biochem. Biophys. Res. Commun. *443*, 1195–1199.

Bähre, H., Hartwig, C., Munder, A., Wolter, S., Stelzer, T., Schirmer, B., Beckert, U., Frank, D.W., Tümmler, B., Kaever, V., and Seifert, R. (2015). cCMP and cUMP occur in vivo. Biochem. Biophys. Res. Commun. *460*, 909–914.

Baym, M., Kryazhimskiy, S., Lieberman, T.D., Chung, H., Desai, M.M., and Kishony, R. (2015). Inexpensive multiplexed library preparation for megabase-sized genomes. PLoS ONE *10*, e0128036.

Beckert, U., Grundmann, M., Wolter, S., Schwede, F., Rehmann, H., Kaever, V., Kostenis, E., and Seifert, R. (2014). cNMP-AMs mimic and dissect bacterial nucleotidyl cyclase toxin effects. Biochem. Biophys. Res. Commun. *451*, 497–502.

Bernheim, A., and Sorek, R. (2020). The pan-immune system of bacteria: antiviral defence as a community resource. Nat. Rev. Microbiol. *18*, 113–119.

Bernheim, A., Millman, A., Ofir, G., Meitav, G., Avraham, C., Shomar, H., Rosenberg, M.M., Tal, N., Melamed, S., Amitai, G., and Sorek, R. (2021). Prokaryotic viperins produce diverse antiviral molecules. Nature *589*, 120–124.

Burroughs, A.M., Zhang, D., Schäffer, D.E., Iyer, L.M., and Aravind, L. (2015). Comparative genomic analyses reveal a vast, novel network of nucleotide-centric systems in biological conflicts, immunity and signaling. Nucleic Acids Res. *43*, 10633–10654.

Chan, P.J. (1987). The effect of cyclic cytidine 3′,5′-monophosphate (cCMP) on the in vitro development, hatching and attachment of the mouse blastocyst. Experientia *43*, 929–930.

Chen, V.B., Arendall, W.B., 3rd, Headd, J.J., Keedy, D.A., Immormino, R.M., Kapral, G.J., Murray, L.W., Richardson, J.S., and Richardson, D.C. (2010). MolProbity: all-atom structure validation for macromolecular crystallography. Acta Crystallogr. D Biol. Crystallogr. *66*, 12–21.

Chen, I.A., Chu, K., Palaniappan, K., Pillay, M., Ratner, A., Huang, J., Huntemann, M., Varghese, N., White, J.R., Seshadri, R., et al. (2019). IMG/M v.5.0: an integrated data management and comparative analysis system for microbial genomes and microbiomes. Nucleic Acids Res. *47* (D1), D666–D677.

Cohen, D., Melamed, S., Millman, A., Shulman, G., Oppenheimer-Shaanan, Y., Kacen, A., Doron, S., Amitai, G., and Sorek, R. (2019). Cyclic GMP-AMP signalling protects bacteria against viral infection. Nature *574*, 691–695.

Crooks, G.E., Hon, G., Chandonia, J.M., and Brenner, S.E. (2004). WebLogo: a sequence logo generator. Genome Res. *14*, 1188–1190.

Deatherage, D.E., and Barrick, J.E. (2014). Identification of mutations in laboratory-evolved microbes from next-generation sequencing data using breseq. Methods Mol. Biol. *1151*, 165–188.

Dodds, P.N., and Rathjen, J.P. (2010). Plant immunity: towards an integrated view of plant-pathogen interactions. Nat. Rev. Genet. *11*, 539–548.

Doron, S., Melamed, S., Ofir, G., Leavitt, A., Lopatina, A., Keren, M., Amitai, G., and Sorek, R. (2018). Systematic discovery of antiphage defense systems in the microbial pangenome. Science *359*, eaar4120.

Eaglesham, J.B., Pan, Y., Kupper, T.S., and Kranzusch, P.J. (2019). Viral and metazoan poxins are cGAMP-specific nucleases that restrict cGAS-STING signalling. Nature *566*, 259–263.

Emsley, P., and Cowtan, K. (2004). Coot: model-building tools for molecular graphics. Acta Crystallogr. D Biol. Crystallogr. *60*, 2126–2132.

Gaion, R.M., and Krishna, G. (1979). Cytidylate cyclase: the product isolated by the method of Cech and Ignarro is not cytidine 3′,5′-monophosphate. Biochem. Biophys. Res. Commun. *86*, 105–111.

Gomelsky, M., and Galperin, M.Y. (2013). Bacterial second messengers, cGMP and c-di-GMP, in a quest for regulatory dominance. EMBO J. *32*, 2421–2423.

Green, J., Stapleton, M.R., Smith, L.J., Artymiuk, P.J., Kahramanoglou, C., Hunt, D.M., and Buxton, R.S. (2014). Cyclic-AMP and bacterial cyclic-AMP receptor proteins revisited: adaptation for different ecological niches. Curr. Opin. Microbiol. *18*, 1–7.

Hanoune, J., and Defer, N. (2001). Regulation and role of adenylyl cyclase isoforms. Annu. Rev. Pharmacol. Toxicol. *41*, 145–174.

Huet, A., Duda, R.L., Boulanger, P., and Conway, J.F. (2019). Capsid expansion of bacteriophage T5 revealed by high resolution cryoelectron microscopy. Proc. Natl. Acad. Sci. USA *116*, 21037–21046.

Jiang, Y., Liu, T., Lee, C.H., Chang, Q., Yang, J., and Zhang, Z. (2020). The NAD^+-mediated self-inhibition mechanism of pro-neurodegenerative SARM1. Nature *588*, 658–663.

Jumper, J., Evans, R., Pritzel, A., Green, T., Figurnov, M., Ronneberger, O., Tunyasuvunakool, K., Bates, R., Žídek, A., Potapenko, A., et al. (2021). Highly accurate protein structure prediction with AlphaFold. Nature *596*, 583–589.

Kabsch, W. (2010). XDS. Acta Crystallogr. D Biol. Crystallogr. *66*, 125–132.

Karplus, P.A., and Diederichs, K. (2012). Linking crystallographic model and data quality. Science *336*, 1030–1033.

Katoh, K., Rozewicki, J., and Yamada, K.D. (2019). MAFFT online service: multiple sequence alignment, interactive sequence choice and visualization. Brief. Bioinform. *20*, 1160–1166.

Kazlauskiene, M., Kostiuk, G., Venclovas, Č., Tamulaitis, G., and Siksnys, V. (2017). A cyclic oligonucleotide signaling pathway in type III CRISPR-Cas systems. Science *357*, 605–609.

Kelley, L.A., Mezulis, S., Yates, C.M., Wass, M.N., and Sternberg, M.J.E. (2015). The Phyre2 web portal for protein modeling, prediction and analysis. Nat. Protoc. *10*, 845–858.

Khannpnavar, B., Mehta, V., Qi, C., and Korkhov, V. (2020). Structure and function of adenylyl cyclases, key enzymes in cellular signaling. Curr. Opin. Struct. Biol. *63*, 34–41.

Lee, T.S., Krupa, R.A., Zhang, F., Hajimorad, M., Holtz, W.J., Prasad, N., Lee, S.K., and Keasling, J.D. (2011). BglBrick vectors and datasheets: A synthetic biology platform for gene expression. J. Biol. Eng. *5*, 12.

Letunic, I., and Bork, P. (2019). Interactive Tree Of Life (iTOL) v4: recent updates and new developments. Nucleic Acids Res. *47* (W1), W256–W259.

Liebschner, D., Afonine, P.V., Baker, M.L., Bunkóczi, G., Chen, V.B., Croll, T.I., Hintze, B., Hung, L.W., Jain, S., McCoy, A.J., et al. (2019). Macromolecular structure determination using X-rays, neutrons and electrons: recent developments in Phenix. Acta Crystallogr. D Struct. Biol. *75*, 861–877.

Lincoln, T.M. (1989). Cyclic GMP and mechanisms of vasodilation. Pharmacol. Ther. *41*, 479–502.

Linder, J.U. (2005). Substrate selection by class III adenylyl cyclases and guanylyl cyclases. IUBMB Life *57*, 797–803.

Linder, J.U. (2010). cGMP production in bacteria. Mol. Cell. Biochem. *334*, 215–219.

Linder, J., Hupfeld, E., Weyand, M., Steegborn, C., and Moniot, S. (2020). Crystal structure of a class III adenylyl cyclase-like ATP-binding protein from Pseudomonas aeruginosa. J. Struct. Biol. *211*, 107534.

Lopatina, A., Tal, N., and Sorek, R. (2020). Abortive Infection: Bacterial Suicide as an Antiviral Immune Strategy. Annu. Rev. Virol. *7*, 371–384.

Lorenz, R., Bernhart, S.H., Höner Zu Siederdissen, C., Tafer, H., Flamm, C., Stadler, P.F., and Hofacker, I.L. (2011). ViennaRNA Package 2.0. Algorithms Mol. Biol. *6*, 26.

Lowey, B., Whiteley, A.T., Keszei, A.F.A., Morehouse, B.R., Mathews, I.T., Antine, S.P., Cabrera, V.J., Kashin, D., Niemann, P., Jain, M., et al. (2020). CBASS Immunity Uses CARF-Related Effectors to Sense 3′-5′- and 2′-5′-Linked Cyclic Oligonucleotide Signals and Protect Bacteria from Phage Infection. Cell *182*, 38–49.e17.

Mazzocco, A., Waddell, T.E., Lingohr, E., and Johnson, R.P. (2009). Enumeration of bacteriophages using the small drop plaque assay system. Methods Mol. Biol. *501*, 81–85.

Millman, A., Melamed, S., Amitai, G., and Sorek, R. (2020a). Diversity and classification of cyclic-oligonucleotide-based anti-phage signalling systems. Nat. Microbiol. *5*, 1608–1615.

Millman, A., Bernheim, A., Stokar-Avihail, A., Fedorenko, T., Voichek, M., Leavitt, A., Oppenheimer-Shaanan, Y., and Sorek, R. (2020b). Bacterial Retrons Function In Anti-Phage Defense. Cell *183*, 1551–1561.e12.

Morehouse, B.R., Govande, A.A., Millman, A., Keszei, A.F.A., Lowey, B., Ofir, G., Shao, S., Sorek, R., and Kranzusch, P.J. (2020). STING cyclic dinucleotide sensing originated in bacteria. Nature *586*, 429–433.

Newton, R.P., Salih, S.G., Salvage, B.J., and Kingston, E.E. (1984). Extraction, purification and identification of cytidine 3′,5′-cyclic monophosphate from rat tissues. Biochem. J. *221*, 665–673.

Ofir, G., Herbst, E., Baroz, M., Cohen, D., Millman, A., Doron, S., Tal, N., Malheiro, D.B.A., Malitsky, S., Amitai, G., et al. (2021). Antiviral activity of bacterial TIR domains via signaling molecules that trigger cell death. bioRxiv. https://doi.org/10.1101/2021.01.06.425286.

Pastan, I., and Perlman, R. (1970). Cyclic adenosine monophosphate in bacteria. Science *169*, 339–344.

Price, M.N., Dehal, P.S., and Arkin, A.P. (2009). FastTree: computing large minimum evolution trees with profiles instead of a distance matrix. Mol. Biol. Evol. *26*, 1641–1650.

Rauch, A., Leipelt, M., Russwurm, M., and Steegborn, C. (2008). Crystal structure of the guanylyl cyclase Cya2. Proc. Natl. Acad. Sci. USA *105*, 15720–15725.

Rohou, A., and Grigorieff, N. (2015). CTFFIND4: Fast and accurate defocus estimation from electron micrographs. J. Struct. Biol. *192*, 216–221.

Ryu, M.H., Youn, H., Kang, I.H., and Gomelsky, M. (2015). Identification of bacterial guanylate cyclases. Proteins *83*, 799–804.

Seifert, R. (2015). cCMP and cUMP: emerging second messengers. Trends Biochem. Sci. *40*, 8–15.

Seifert, R. (2017). cCMP and cUMP across the tree of life: From cCMP and cUMP generators to cCMP- and cUMP-regulated cell functions. In Handbook of Experimental Pharmacology, R. Seifert, ed. (Springer), pp. 3–23.

Seifert, R., Beste, K., Burhenne, H., Voigt, U., Wolter, S., Hammerschmidt, A., Reinecke, D., Sandner, P., Pich, A., Schwede, F., et al. (2011). Cyclic CMP and cyclic UMP: new (old) second messengers. BMC Pharmacol. *11*, O34.

Sievers, F., and Higgins, D.G. (2018). Clustal Omega for making accurate alignments of many protein sequences. Protein Sci. *27*, 135–145.

Söding, J., Biegert, A., and Lupas, A.N. (2005). The HHpred interactive server for protein homology detection and structure prediction. Nucleic Acids Res. *33*, W244-8.

Sporny, M., Guez-Haddad, J., Lebendiker, M., Ulisse, V., Volf, A., Mim, C., Isupov, M.N., and Opatowsky, Y. (2019). Structural Evidence for an Octameric Ring Arrangement of SARM1. J. Mol. Biol. *431*, 3591–3605.

Steegborn, C. (2014). Structure, mechanism, and regulation of soluble adenylyl cyclases - similarities and differences to transmembrane adenylyl cyclases. Biochim. Biophys. Acta *1842* (12 Pt B), 2535–2547.

Steinegger, M., and Söding, J. (2017). MMseqs2 enables sensitive protein sequence searching for the analysis of massive data sets. Nat. Biotechnol. *35*, 1026–1028.

Stryer, L. (1986). Cyclic GMP cascade of vision. Annu. Rev. Neurosci. *9*, 87–119.

Tesmer, J.J.G., Sunahara, R.K., Johnson, R.A., Gosselin, G., Gilman, A.G., and Sprang, S.R. (1999). Two-metal-Ion catalysis in adenylyl cyclase. Science *285*, 756–760.

Torarinsson, E., and Lindgreen, S. (2008). WAR: Webserver for aligning structural RNAs. Nucleic Acids Res. *36*, W79-84.

Waterhouse, A.M., Procter, J.B., Martin, D.M.A., Clamp, M., and Barton, G.J. (2009). Jalview Version 2–a multiple sequence alignment editor and analysis workbench. Bioinformatics *25*, 1189–1191.

Weiss, M.S. (2001). Global indicators of X-ray data quality. J. Appl. Crystallogr. *34*, 130–135.

Whiteley, A.T., Eaglesham, J.B., de Oliveira Mann, C.C., Morehouse, B.R., Lowey, B., Nieminen, E.A., Danilchanka, O., King, D.S., Lee, A.S.Y., Mekalanos, J.J., and Kranzusch, P.J. (2019). Bacterial cGAS-like enzymes synthesize diverse nucleotide signals. Nature *567*, 194–199.

Zhou, W., Whiteley, A.T., de Oliveira Mann, C.C., Morehouse, B.R., Nowak, R.P., Fischer, E.S., Gray, N.S., Mekalanos, J.J., and Kranzusch, P.J. (2018). Structure of the Human cGAS-DNA Complex Reveals Enhanced Control of Immune Surveillance. Cell *174*, 300–311.e11.

Zivanov, J., Nakane, T., and Scheres, S.H.W. (2020). Estimation of high-order aberrations and anisotropic magnification from cryo-EM data sets in *RELION*-3.1. IUCrJ *7*, 253–267.

Please cite this article in press as: Tal et al., Cyclic CMP and cyclic UMP mediate bacterial immunity against phages, Cell (2021), https://doi.org/10.1016/j.cell.2021.09.031

STAR★METHODS

KEY RESOURCES TABLE

REAGENT or RESOURCE	SOURCE	IDENTIFIER
Bacterial and virus strains		
E. coli K-12 MG1655	American Type Culture Collection (ATCC)	ATCC 47076
E. coli BL21-DE3 RIL	Agilent	Cat#230245
Phage Lambda-vir	U. Qimron	N/A
Phage SECPhi17	Doron et al., 2018	N/A
Phage SECphi18	Doron et al., 2018	N/A
Phage SECphi27	Doron et al., 2018	N/A
Phage SECphi6	Millman et al., 2020b	N/A
Phage SECphi4	Millman et al., 2020b	N/A
Phage P1	U. Qimron	N/A
Phage T2	German Collection of Microorganisms and Cell Cultures GmbH (DSMZ)	DSM 16352
Phage T4	U. Qimron	N/A
Phage T5	U. Qimron	N/A
Phage T6	German Collection of Microorganisms and Cell Cultures GmbH (DSMZ)	DSM 4622
Phage T7	U. Qimron	N/A
Phage T5 – pb8 mutant n.1	This paper	N/A
Phage T5 – pb8 mutant n.4	This paper	N/A
Phage T5 – pb8 mutant n.9	This paper	N/A
Chemicals, peptides, and recombinant proteins		
[α-^{32}P] ATP	Perkin Elmer	Cat#BLU003H250UC
[α-^{32}P] GTP	Perkin Elmer	Cat#BLU006H250UC
[α-^{32}P] UTP	Perkin Elmer	Cat#BLU007H250UC
[α-^{32}P] CTP	Perkin Elmer	Cat#BLU008H250UC
NTPs (ATP, GTP, UTP, CTP)	New England Biolabs	Cat#N0450S
3′,5′-cCMP	Biolog	Cat#C 001
3′,5′-cUMP	Biolog	Cat#U 001
3′,5′-cAMP	Biolog	Cat#A001S
3′,5′-cGMP	Biolog	Cat#G001
Nicotinamide adenine dinucleotide (NAD$^+$)	Sigma-Aldrich	Cat#N0632
ε-NAD$^+$ Nicotinamide 1,N^6-ethenoadenine dinucleotide (ε-NAD$^+$)	Sigma-Aldrich	Cat#N2630
Adenosine 5′-diphosphoribose (ADPR)	Sigma-Aldrich	Cat#A0752
Nicotinamide (NAM)	Sigma-Aldrich	Cat#N3376
membrane stain FM4-64	Thermo Fisher Scientific	Cat#T13320
DNA stain DAPI	Sigma-Aldrich	Cat#D9542
Ni-NTA Agarose	QIAGEN	Cat#30250
HiLoad 16/600 Superdex 75 PG	GE Healthcare	Cat#28989333
HiLoad 16/600 Superdex 200 PG	GE Healthcare	Cat#28989336
Zorbax Bonus-RP HPLC Column	Agilent	Cat#863668-901
Silica Gel-60 F_{254} glass-backed TLC plate	MilliporeSigma	Cat#M1057290001
Alkaline Phosphatase, Calf Intestinal (CIP)	New England Biolabs	Cat#M0290S
SYPRO Orange Fluorescent Dye	ThermoFisher	Cat#S6650

(*Continued on next page*)

Please cite this article in press as: Tal et al., Cyclic CMP and cyclic UMP mediate bacterial immunity against phages, Cell (2021), https://doi.org/10.1016/j.cell.2021.09.031

Continued

REAGENT or RESOURCE	SOURCE	IDENTIFIER
HEPES	VWR	Cat#97061-824
Tris base	VWR	Cat#97062-416
PEG 3350	Sigma-Aldrich	Cat#202444
Ammonium acetate	ThermoFisher	Cat#A639
Imidazole	VWR	Cat#97065-016
Tris[-2carboxyethyl] phosphine hydrochloride (TCEP)	GoldBio	Cat#TCEP50
Dithiothreitol (DTT)	GoldBio	Cat#DTT25
*Ec*PycC recombinant protein, and mutants as described	This paper	N/A
*Bc*PycC recombinant protein, and mutants as described	This paper	N/A
*Pa*PycC recombinant protein	This paper	N/A
*Rs*PycC recombinant protein	This paper	N/A
*Rsm*PycC recombinant protein	This paper	N/A
*Tp*PycC recombinant protein	This paper	N/A
*Gm*PycC recombinant protein	This paper	N/A
*Pt*PycC recombinant protein	This paper	N/A
*Me*PycC recombinant protein	This paper	N/A
*Sa*PycC recombinant protein	This paper	N/A
*Ec*303145PycC recombinant protein	This paper	N/A
*Bc*PycTIR recombinant protein	This paper	N/A
Critical commercial assays		
DNeasy blood and tissue kit	QIAGEN	Cat #69504
Nextera DNA Library Prep Kit	Illumina	Cat#15027865, Cat#15027866
RNase A (within QIAprep Spin Miniprep Kit)	QIAGEN	Cat# 27106
DNase-I	Merck	Cat#11284932001
Deposited data		
Crystal structure of *Bc*PycC cUMP synthase	This paper	PDB: 7R65
Oligonucleotides		
Primers, see Table S4	This paper	N/A
Recombinant DNA		
pBbS8k-RFP	Lee et al., 2011	Addgene Cat#35276
pSG1	Doron et al., 2018	N/A
pBAD-GFP	Thermo Fisher Scientific	Cat #43001
E. coli E831 Pycsar	Genscript	N/A
E. coli E831 Pycsar cyclase mutant F100A	Genscript	N/A
E. coli E831 Pycsar cyclase mutant R142A	Genscript	N/A
E. coli E831 Pycsar cyclase mutant M144A	Genscript	N/A
E. coli E831 Pycsar cyclase mutant D146A	Genscript	N/A
E. coli E831 Pycsar delta AGS-C	Genscript	N/A
E. coli 303145 Pycsar	Genscript	N/A
X. perforans GEV1001 Pycsar	Genscript	N/A
pBbS8k-pb8	This paper	N/A
pET16-6 × His-SUMO2	Zhou et al., 2018	N/A
pET16-6 × His-MBP-SUMO2	This paper	N/A
Software and algorithms		
The Integrated Microbial Genomes (IMG)	Chen et al., 2019	https://img.jgi.doe.gov/m/

(*Continued on next page*)

Please cite this article in press as: Tal et al., Cyclic CMP and cyclic UMP mediate bacterial immunity against phages, Cell (2021), https://doi.org/10.1016/j.cell.2021.09.031

Continued

REAGENT or RESOURCE	SOURCE	IDENTIFIER
MMseqs2	Steinegger and Söding, 2017	https://github.com/soedinglab/mmseqs2
RNAfold WebServer	Lorenz et al., 2011	http://rna.tbi.univie.ac.at/cgi-bin/RNAWebSuite/RNAfold.cgi
BLASTclust from the BLAST NCBI package	Altschul et al., 1990	https://ftp.ncbi.nlm.nih.gov/blast/executables/legacy.NOTSUPPORTED/2.2.26/
WAR web server	Torarinsson and Lindgreen, 2008	https://rth.dk/resources/war
HHpred	Söding et al., 2005	https://toolkit.tuebingen.mpg.de/tools/hhpred
FastTree	Price et al., 2009	http://microbesonline.org/fasttree
iTOL	Letunic and Bork, 2019	https://itol.embl.de/
Breseq (version 0.34.1)	Deatherage and Barrick, 2014	http://barricklab.org/twiki/bin/view/Lab/ToolsBacterialGenomeResequencing
Prism v9.0d	GraphPad software	https://www.graphpad.com/scientific-software/prism/
Pymol v2.4.0	Schrödinger, LLC	https://pymol.org/2/
Coot v0.8.9.3-pre	Emsley and Cowtan, 2004	https://www2.mrc-lmb.cam.ac.uk/personal/pemsley/coot/
Phenix v1.18.2-3874	Liebschner et al., 2019	https://phenix-online.org/
ImageJ	NIH	https://login.ezp-prod1.hul.harvard.edu/login?qurl=https://imagej.nih.gov%2fij%2findex.html
ImageQuant TL v8.2.0	GE Healthcare	http://www.cytivalifesciences.com/en/us/shop/protein-analysis/molecular-imaging-for-proteins/imaging-software/imagequant-tl-8-2-image-analysis-software-p-09518
Jalview v2.11.1.4	Waterhouse et al., 2009	http://www.jalview.org
MAFFT v7	Katoh et al., 2019	https://mafft.cbrc.jp/alignment/server/

RESOURCE AVAILABILITY

Lead contact

Further information and requests for resources and reagents should be directed to the Lead Contact, Rotem Sorek (rotem.sorek@weizmann.ac.il).

Materials availability

This study did not generate new unique reagents.

Data and code availability

Crystal structure of *Bc*PycC was deposited at the protein data base under identifier PDB: 7R65, and is publicly available as of the date of publication. All additional data reported in this paper will be shared by the lead contact upon request. This paper does not report original code.

EXPERIMENTAL MODEL AND SUBJECT DETAILS

Bacterial strains and phages

E. coli strain MG1655 (ATCC 47076) was grown in MMB (LB + 0.1 mM $MnCl_2$ + 5 mM $MgCl_2$, with or without 0.5% agar) at 37°C or room temperature (RT). Whenever applicable, media were supplemented with ampicillin (100 μg mL^{-1}) or kanamycin (50 μg mL-1), to ensure the maintenance of plasmids. Infection was performed in MMB media at 37°C or room temperature as detailed in each section. *E. coli* BL21-DE3 was grown in MDG (0.5% glucose, 25 mM Na_2HPO_4, 25 mM KH_2PO_4, 50 mM NH_4Cl, 5 mM Na_2SO_4, 2 mM $MgSO_4$, 0.25% aspartic acid, 100 mg mL−1 ampicillin, 34 mg mL−1 chloramphenicol, and trace metals). Overnight MDG cultures were used to inoculate cultures of M9ZB media (0.5% glycerol, 1% Cas-amino Acids, 47.8 mM Na_2HPO_4, 22 mM

Please cite this article in press as: Tal et al., Cyclic CMP and cyclic UMP mediate bacterial immunity against phages, Cell (2021), https://doi.org/10.1016/j.cell.2021.09.031

KH_2PO_4, 18.7 mM NH_4Cl, 85.6 mM NaCl, 2 mM $MgSO_4$, 100 mg mL−1 ampicillin, 34 mg mL−1 chloramphenicol, and trace metals, as described previously (Zhou et al., 2018)), which were grown and harvested for each experiment. Phages used in this study are listed in Table S3 and in the Key resources table.

METHOD DETAILS

Detection of cNMP cyclase systems in defense islands

Protein sequences of all genes in 38,167 bacterial and archaeal genomes were downloaded from the Integrated Microbial Genomes (IMG) database (Chen et al., 2019) in October 2017 and clustered into protein families as described in (Millman et al., 2020a). Defense scores were calculated as previously described (Doron et al., 2018), recording the fraction of genes in each cluster that have known defense genes in their genomic environment spanning 10 genes upstream and downstream the inspected gene. For each cluster an average number of known defense genes in the genomic environment of all members was also calculated. Clusters where the most common pfam annotation was PF00211, with average protein size > 200 aa, defense score > 0.35 and average number of known defense genes in the environment > 0.8 were included in the family of cyclase genes studied here.

Plasmid and strain construction

E. coli E831, *E. coli* 303145 and *X. perforans* GEV1001 Pycsar systems used in this study were synthesized by Genscript Corp. and cloned into the pSG1 plasmid (Doron et al., 2018) with their native promoters, or into the pBAD plasmid (Thermofisher, cat. #43001) (Table S4) as previously described (Bernheim et al., 2021; Doron et al., 2018). Mutants of the cyclase gene of *E. coli* E831 were also synthesized and cloned by Genscript. All synthesized sequences are presented in Table S4. A pBAD plasmid containing the cCMP cyclase of *E. coli* E831 was cloned using primers NT148 and NT149 listed in Table S4.

Plaque assays

Phages were propagated by picking a single phage plaque into a liquid culture of *E. coli* MG1655 grown at 37°C to OD_{600} of 0.3 in MMB medium until culture collapse. The culture was then centrifuged for 10 min at 3200 × g and the supernatant was filtered through a 0.2 μm filter to remove remaining bacteria and bacterial debris. Lysate titer was determined using the small drop plaque assay method as described in (Mazzocco et al., 2009). In brief, *E. coli* MG1655 cells were grown overnight at 37°C. Then 300 μL of the bacterial culture was mixed with 30 mL melted MMB agar (LB + 0.1 mM MnCl2 + 5 mM MgCl2 + 0.5% agar and left to dry for 1 h at room temperature. 10-fold serial dilutions in MMB were performed for each of the tested phages and 10 μL drops were put on the bacterial layer. Plates were incubated overnight at room temperature. Plaque forming units (PFUs) were determined by counting the derived plaques after overnight incubation and lysate titer was determined by calculating PFUs per mL.

Plaque assays were performed as previously described in Mazzocco et al. (2009). Bacteria (*E. coli* MG1655 with the pSG1 plasmid containing the Pycsar system from *E. coli* E831 and *E. coli* 303145 or the pBAD plasmid with the system from *X. perforans* GEV1001) and negative control (*E. coli* MG1655 with an empty pSG1 vector or pBAD-GFP) were grown overnight at 37°C. Then 300 μL of the bacterial culture was mixed with 30 mL melted MMB agar (LB + 0.1 mM $MnCl_2$ + 5 mM $MgCl_2$ + 0.5% agar, with or without 0.2% arabinose, as described in Table S4) and left to dry for 1 h at room temperature. 10-fold serial dilutions in MMB were performed for each of the tested phages and 10 μL drops were put on the bacterial layer. Plates were incubated overnight at room temperature. Plaque forming units (PFUs) were determined by counting the derived plaques after overnight incubation.

Infection in liquid culture

Overnight cultures of bacteria harboring the Pycsar system (*E. coli* MG1655 with a pSG1 plasmid containing the system from *E. coli* E831 or a pBAD plasmid containing the system from *X. perforans* GEV1001) or negative control (*E. coli* MG1655 with a an empty pSG1 plasmid or a pBAD-GFP plasmid) were diluted 1:100 in MMB medium. For pBAD containing cultures, 0.2% arabinose was added. Cells were incubated at 37°C while shaking at 200 rpm until early log phase (OD_{600} 0.3). 180 μL of the bacterial culture were transferred into wells in a 96-well plate containing 20 μL of phage lysate for a final MOI of 2 or 0.02, or phage buffer (50 mM Tris-HCl pH 7.4, 100 mM $MgCl_2$, 10 mM NaCl) for uninfected control. Infections were performed in triplicates from overnight cultures prepared from three separate colonies. Plates were incubated at 37°C with shaking in a TECAN Infinite200 plate reader and OD_{600} was followed with measurement every 10 min.

cCMP/cUMP supplementation assays

Overnight cultures of bacteria harboring the system (*E. coli* MG1655 with a pBAD plasmid containing the system from *E. coli* E831 or a pBAD plasmid containing the system from *X. perforans* GEV1001) or negative control (*E. coli* MG1655 with a pBAD-GFP plasmid) were diluted 1:100 in MMB medium with 0.2% arabinose. Cells were incubated at 37°C while shaking at 200 rpm until early log phase (OD_{600} 0.3). 180 μL of the bacterial culture were transferred into wells in a 96-well plate containing 20 μL of different concentrations of 3′,5′-cCMP, 3′,5′-cUMP or ultrapure water as a control. Plates were incubated at 37°C with shaking in a TECAN Infinite200 plate reader and OD_{600} was followed with measurement every 10 min.

Please cite this article in press as: Tal et al., Cyclic CMP and cyclic UMP mediate bacterial immunity against phages, Cell (2021), https://doi.org/10.1016/j.cell.2021.09.031

Cell lysate preparation

Overnight cultures of *E. coli* harboring the Pycsar systems and negative controls were diluted 1:100 in 250 mL MMB medium (with or without arabinose, as described in Table S4) and grown at 37°C (250 rpm) until reaching OD_{600} of 0.3. The cultures containing the cyclase from *E. coli* E831 were infected by T5, and cells containing the Pycsar system from *X. perforans* GEV1001 were infected by T7 at a final MOI of 2. Following the addition of phage, at 15, 30, and 40 min post infection for T5- (WT or mutant) infected cells, or at 5 and 10 min post infection for T7-infected cells, plus an uninfected control sample. 50 mL samples were taken and centrifuged for 5 min at 3200 × g. The culture pellets were flash frozen using dry ice and ethanol. The pellets were re-suspended in 600 μl of 100 mM phosphate buffer at pH 8 and supplemented with 4 mg mL^{-1} lysozyme. The samples were then transferred to a FastPrep Lysing Matrix B 2 mL tube (MP Biomedicals cat. #116911100) and lysed using a FastPrep bead beater for 40 s at 6 m s^{-1} (two cycles). Tubes were then centrifuged at 4°C for 15 min at 15,000 × g. Supernatant was transferred to Amicon Ultra-0.5 Centrifugal Filter Unit 3 kDa (Merck Millipore cat. #UFC500396) and centrifuged for 45 min at 4°C at 12,000 × g. Filtrate was taken and used for LC-MS/MS analysis.

Quantification of nucleotides by HPLC-MS/MS

Cell lysates were prepared as described above and analyzed by LC-MS/MS. Quantification of nucleotides was carried out using an Acquity I-class UPLC system coupled to Xevo TQ-S triple quadrupole mass spectrometer (both Waters, US). The UPLC was performed using an Atlantis Premier BEH C18 AX column with the dimension of 2.1 × 100 mm and particle size of 1.7 μm (Waters). Mobile phase A was 20 mM ammonium formate at pH 3 and acetonitrile was mobile phase B. The flow rate was kept at 300 μl min^{-1} consisting of a 2 min hold at 2% B, followed by linear gradient increase to 100% B during 5 min. The column temperature was set at 25°C and an injection volume of 1 μl. An electrospray ionization interface was used as ionization source. Analysis was performed in positive ionization mode. Metabolites were detected using multiple-reaction monitoring, using argon as the collision gas. Quantification was made using standard curve in 0–10 μM concentration range. $^{15}N_5$-adenosine 5′-monophosphate (Sigma) was added to standards and samples as internal standard (0.5 μM). TargetLynx (Waters) was used for data analysis.

Mass spectrometry of *in vitro* reactions

20 μL reactions containing purified *Ec*PycC or *Bc*PycC with 500 μM CTP or UTP were incubated at 37°C overnight in buffer (50 mM CAPSO pH 9.4, 100 mM KCl, 10 mM $MgCl_2$, 1 mM $MnCl_2$), heat inactivated at 95°C for 2 min, diluted to 200 μL with RNase-free water and filtered through 10 kDa cutoff Amicon™ Ultra centrifuge filters (Millipore). Sample analysis by high-resolution LC-MS/MS was carried out by MS-Omics (Vedbæk).

Thermal denaturation assay

*Ec*PycC (wild-type or D102A mutant) was added at a final concentration of 20 μM with 3 × SYPRO Orange Dye in a buffer of 100 mM KCl, 20 mM HEPES-KOH pH 7.5. Samples were heated from 20 to 95°C over the course of 2 h using a qPCR CFX96 thermocycler (Biorad) and fluorescence in the HEX channel was measured every 0.5°C. The first derivative of each fluorescence curve was calculated, and the melting temperature was identified as the peak of each derivative curve.

Isolation of mutant phages

To isolate mutant phages that escape defense, phages were plated on bacteria expressing the Pycsar system (*E. coli* E831) using the double-layer plaque assay (Mazzocco et al., 2009). For this, 100 μL of bacterial cells grown in MMB to an OD_{600} of 0.3 were mixed with 100 μL of T5 phage, and left at room temperature for 10 min. 5 mL of pre-melted 0.3% MMB were added and the mixture was poured onto a bottom layer of 1.1% MMB. The double layer plates were incubated overnight at 37°C (mutants #1–10) or room temperature (mutants #11–17) and single plaques were picked into 90 μl phage buffer.

For mutants #10 and #17, instead of picking single plaques, the entire top layer was scraped into 2 mL of phage buffer to enrich for phages that escape Pycsar defense. Phages were left for 1 h at room temperature during which the phages were mixed several times by vortex to release them from the agar into the phage buffer. The phages were centrifuged at 3200 × g for 10 min to remove agar and bacterial cells, and the supernatant was transferred to a new tube.

In order to test the phages for the ability to escape from the defense system, the small drop plaque assay was used (Mazzocco et al., 2009). 300 mL of an overnight culture of either *E. coli* E831 or *E. coli* MG1655 with plasmid pSG1 were mixed with 30 mL melted MMB 0.3% agar and left to dry for 1 h at room temperature. 10-fold serial dilutions in phage buffer were performed for the ancestor T5 phage (WT phage used for the original double layer plaque assay) and the T5 phage mutants #1–17 isolated from plaques formed on the strain expressing the defense genes. 10 μL drops of the phage were put on the bacterial layer. The plates were incubated overnight at 37°C or room temperature for mutants #1–10 and #11–17 respectively.

Amplification of mutant phages

Isolated phages for which there was decreased defense compared to the ancestor phage were further propagated by picking a single plaque formed on *E. coli* MG1655 containing the *E. coli* E831 Pycsar system in the small drop plaque assay into a liquid culture of the same strain, which was grown at 37°C in MMB with shaking at 200 rpm to an OD_{600} of 0.3. The phages were incubated with the bacteria at 37°C with shaking at 200 rpm for 3 h, and then an additional 9 mL of bacterial culture grown to OD_{600} of 0.3 in MMB was added,

Please cite this article in press as: Tal et al., Cyclic CMP and cyclic UMP mediate bacterial immunity against phages, Cell (2021), https://doi.org/10.1016/j.cell.2021.09.031

and incubated for 3 additional hours in the same conditions. The lysates were then centrifuged at 3200 × g for 10 min and the supernatant was filtered through a 0.2 μm filter to remove remaining bacteria. Phage titer was then checked using the small drop plaque assay on the negative control strain as described above.

Sequencing and genome analysis of phage mutants

High titer phage lysates (> 10^7 PFU/mL) of the ancestor phage and isolated phage mutants were used for DNA extraction. 0.5 mL of phage lysate was treated with DNase-I (Merck cat #11284932001) added to a final concentration of 20 μg mL^{-1} and incubated at 37°C for 1 h to remove bacterial DNA. DNA was extracted using the QIAGEN DNeasy blood and tissue kit (cat. #69504) starting from a proteinase-K treatment to degrade the phage capsids. Libraries were prepared for Illumina sequencing using a modified Nextera protocol as previously described (Baym et al., 2015). Following sequencing on Illumina NextSeq500, reads were aligned to the T5 phage reference genome (GenBank accession number: AY543070) and mutations compared to the reference genome were identified using Breseq (version 0.34.1) with default parameters (Deatherage and Barrick, 2014). Only mutations that occurred in the isolated mutants, but not in the ancestor phage, were considered. Silent mutations within protein coding regions were disregarded as well.

Microscopy of infected cells

E. coli MG1655 cells that contain an inducible pBAD plasmid containing the *E. coli* E831-derived Pycsar or a negative control containing a pBAD-GFP plasmid were grown in MMB medium at 37°C with 0.2% arabinose. When growth reached an OD_{600} of 0.3, 250 μM of cCMP was added to the medium. Sixty min following the addition of cCMP, 500 μL of the samples were centrifuged at 10,000 × g for 2 min at 25°C and resuspended in 5 μL of 1 × phosphate-buffered saline (PBS), supplemented with 1 μg mL^{-1} membrane stain FM4-64 (Thermo Fisher Scientific T-13320) and 2 μg mL^{-1} DNA stain 4,6-diamidino2-phenylindole (DAPI) (Sigma-Aldrich D9542-5MG). Cells were visualized and photographed using an Axioplan2 microscope (ZEISS) equipped with ORCA Flash 4.0 camera (HAMAMATSU). System control and image processing were carried out using Zen software version 2.0 (Zeiss).

Phylogenetic analysis

To generate the phylogenetic tree in Figure 2A the 'clusthash' option of MMseqs2 (Steinegger and Söding, 2017) (release 6-f5a1c) was used to remove protein redundancies (using the '–min-seq-id 0.9' parameter). Sequences that were shorter than 200 amino acids were also removed and HHsearch was used to identify the cyclase domain in each protein sequence. Eight sequences of diguanylate cyclase were added (IMG ID: 2503740511, 2689262325, 2688711941, 2688713579, 2661427045, 2661426508, 2688078042, 2688079262) and were used as an outgroup. Sequences of the cyclase domain were aligned using clustal-omega v.1.2.4 with default parameters (Sievers and Higgins, 2018). FastTree was used to generate a tree from the multiple-sequence alignment using default parameters (Price et al., 2009). iTOL was used for tree visualization (Letunic and Bork, 2019). To generate the sequence motifs of clades B and E, sequences of each clade were aligned using clustal-omega v.1.2.4 with default parameters (Sievers and Higgins, 2018). Weblogo3 (version 2.8.2) was used to generate the motifs for each clade (Crooks et al., 2004).

Fitness assay of mutant pb8 phages

Mutant and WT T5 phages were mixed in a target ratio of approximately 1:1. Overnight cultures of bacteria harboring the defense system (*E. coli* MG1655 with a pSG1 plasmid containing the system from *E. coli* E831 or a negative control strain with an empty vector) were diluted 1:100 in MMB medium. Cells were incubated at 37°C while shaking at 200 rpm until early log phase (OD_{600} of 0.3). System-expressing and control cells were infected with the phage lysate for a final MOI of 0.2, and incubated for 3 h at 37°C while shaking at 200 rpm. Cultures were then centrifuged at 3200 × g for 5 min and phage-containing supernatant was filtered through a 0.2 μm filter to get rid of remaining bacteria. Phage titer was then checked using the small drop plaque assay on the negative control strain as described above. This phage lysate was subsequently used for the infection of a fresh culture of bacteria at an MOI of 0.2 (second passage). The same process was carried out for the third passage. In each of the passages, 0.5 mL of the phage lysate was kept for DNA extraction and sequencing, as detailed above.

Protein expression and purification

BL21-RIL *E. coli* (Agilent) were transformed with plasmid DNA encoding 6 × His-SUMO2-tagged gene expression constructs and plated on MDG-agar plates (0.5% glucose, 25 mM Na_2HPO_4, 25 mM KH_2PO_4, 50 mM NH_4Cl, 5 mM Na_2SO_4, 2 mM $MgSO_4$, 0.25% aspartic acid, 100 mg mL^{-1} ampicillin, 34 mg mL^{-1} chloramphenicol, and trace metals), then colonies were used to inoculate overnight MDG liquid cultures (same components minus the agar). Overnight MDG cultures were used to inoculate cultures of M9ZB media (0.5% glycerol, 1% Cas-amino Acids, 47.8 mM Na_2HPO_4, 22 mM KH_2PO_4, 18.7 mM NH_4Cl, 85.6 mM NaCl, 2 mM $MgSO_4$, 100 mg mL^{-1} ampicillin, 34 mg mL^{-1} chloramphenicol, and trace metals), which were grown and harvested in each experiment as described below. Generally, large scale cultures (1–2 l) expressing constructs were grown for ~5 h at 37°C, then induced with IPTG overnight at 16°C with 230 rpm shaking. For *Bc*PycTIR expression, M9ZB media was supplemented with 10 mM nicotinamide (NAM, Sigma). Selenomethionine-labeled protein for structural determination was prepared as previously described (Eaglesham et al., 2019). Briefly, selenomethionine-labeled *Bc*PycC expression was carried out in modified M9ZB growth media containing 0.4% glucose substituted for Cas-amino acids and supplemented with 1 μg mL^{-1}

Please cite this article in press as: Tal et al., Cyclic CMP and cyclic UMP mediate bacterial immunity against phages, Cell (2021), https://doi.org/10.1016/j.cell.2021.09.031

thiamine. Liter cultures were grown at 37°C to an OD_{600} between 0.5–0.8 before addition of the following amino acids: Leucine, isoleucine, and valine (50 mg L^{-1}, VRW); phenylalanine, lysine, and threonine (100 mg L^{-1}, VWR); selenomethionine (75 mg L^{-1}, Acros Organics). Cultures were grown at 37°C for an additional 20 min and then transferred to ice for 20 min. 0.5 mM IPTG was added and the cultures were incubated overnight at 16°C before harvesting. Cell pellets were washed with PBS, and flash frozen in liquid N_2 prior to short-term storage at −80°C.

Recombinant cyclase enzymes and *Bc*PycTIR were purified as previously described (Morehouse et al., 2020; Zhou et al., 2018). Cell pellets were resuspended and sonicated in lysis buffer (20 mM HEPES-KOH pH 7.5, 400 mM NaCl, 30 mM imidazole, 10% glycerol, supplemented with 1 mM DTT) and purified using Ni-NTA resin (QIAGEN). Resin-bound protein was washed with lysis buffer supplemented to 1 M NaCl and eluted with lysis buffer supplemented to 300 mM imidazole. The eluent was dialyzed into 20 mM HEPES-KOH pH 7.5, 250 mM KCl, 1 mM DTT overnight (16–20 h) while removing the SUMO2 tag with recombinant human SENP2 protease (D364–L589, M497A). Proteins were concentrated using a 10K-cutoff concentrator (Millipore) and either passed back over Ni-NTA resin to remove cleaved 6 × His-SUMO2 and uncleaved protein or further purified by size-exclusion chromatography on a 16/600 Superdex 75 column using the same dialysis buffer system. Proteins were concentrated to > 10 mg mL^{-1}, flash frozen with liquid nitrogen, and stored at −80°C.

Crystallization and structure determination

*Bc*PycC was crystallized using the hanging drop vapor diffusion method at 18°C. Protein was thawed on ice before dilution into 25 mM HEPES-KOH pH 7.5 with 75 mM KCl and 1 mM TCEP bringing the final protein concentration before setting crystallization trays to 8 mg mL^{-1}. Drops were set by mixing 1:1 protein and reservoir solution in 2 μL drops over a 350 μL reservoir in 15-well Easy-Xtal trays (QIAGEN) following sparse screening to identify initial crystal hits. *Bc*PycC crystallized in less than 24 h in 0.1 M ammonium acetate ($NH_4CH_3CO_2$), 0.1 M HEPES-KOH pH 7.5, and 29% PEG-3350. Crystals were harvested and cryoprotected in reservoir solution supplemented with 15% ethylene glycol before plunge freezing in liquid N_2.

X-ray data collection was carried out at the Northeastern Collaborative Access Team beamline 24-ID-E (P30 GM124165), fixed at 12.66 keV and used an Eiger detector (S10OD021527) and the Argonne National Laboratory Advanced Photon Source (DE-AC02-06CH11357). X-ray crystallography data were processed with XDS and AIMLESS (Kabsch, 2010) using the SSRL autoxds script (*A. Gonzalez*, Stanford SSRL). Experimental phase information was determined using data collected from selenomethionine-substituted crystals. 16 anomalous sites (from 4 protein copies in the ASU) were identified with HySS and an initial map was produced using SOLVE/RESOLVE in Phenix (Liebschner et al., 2019). Model building was performed using Coot (Emsley and Cowtan, 2004), then refined in Phenix. Statistics were analyzed as described in Table S5 (Chen et al., 2010; Karplus and Diederichs, 2012; Weiss, 2001).

Thin-layer chromatography analysis of cyclic nucleotide products

Purified cyclases were mixed at a final concentration of 5 μM with 100 μM NTPs and trace radiolabeled α-^{32}P-NTP in 10 μL reactions with 100 mM KCl, 10 mM $MgCl_2$, 1 mM $MnCl_2$, and 50 mM Tris-HCl pH 8.5. These reactions were incubated for 2 h at 37°C and then terminated by treatment with 1 μL of 5 units μL^{-1} Calf Intestinal Phosphatase (CIP, New England Biolabs) for 1 h at 37°C. 1 μL of each reaction was spotted on glass-backed silica-coated thin layer chromatography (TLC) plates (Millipore) and developed for one hour in a solvent system composed of 11:7:2 1-propanol:conc. NH_4OH:water as previously described (Whiteley et al., 2019). TLC plates were dried and then processed by exposing with a phosphor screen followed by imaging with an Amersham Typhoon IP (Cytiva). For optimization experiments reactions were left at 37°C for 25 min then terminated at 85°C for 2 min, and CIP treated for 30 min at 37°C before spotting on TLC.

High-performance liquid chromatography analysis of enzymatic reactions

Cyclic nucleotide synthesis was carried out in 125 μL reactions with 5 μM purified cyclase and 500 μM ATP, CTP, GTP, and UTP in 1 × reaction buffer (100 mM KCl, 10 mM $MgCl_2$, 1 mM $MnCl_2$, 50 mM Tris-HCl pH 8.5), then incubated overnight at 37°C. Reactions were filtered through 10 kDa cutoff Amicon™ Ultra centrifuge filters (Millipore) and injected onto an Agilent 1260 infinity series HPLC. Comparison of major peak products to cyclic nucleotide standards (cAMP [Biolog A 001 S], cGMP [Biolog G 001], cCMP [Biolog C 001], and cUMP [Biolog U 001]) was carried out using a C18 column (Agilent Zorbax Bonus-RP 4.6 × 150 mm, 3.5-micron). The column was heated to 40°C and run at 1 mL min^{-1} with a mobile phase of 50 mM NaH_2PO_4 (pH 6.8 with NaOH) supplemented with 3% acetonitrile. Absorbance signals were monitored at 254 nm.

NADase reactions were carried out in a similar manner with 500 μM NAD^+ (Sigma), 500 nM *Bc*PycTIR, and 0–1mM cNMP ligands. Reactions were incubated for 1 h at 25°C and then filtered prior to HPLC analysis.

Fluorescence plate reader analysis of NADase activity

A plate reader assay was devised to monitor the NADase activity of purified *Bc*PycTIR. Briefly, 30 μL reactions were built in white walled clear bottom 96-well plates. The reactions consisted of buffer (20 mM HEPES-KOH pH 7.5, 100 mM KCl), 1 μM *Bc*PycTIR, a range of 10 nM to 1 mM synthetic cyclic nucleotide ligands, and 500 μM of the fluorescent NAD^+ analog ε-NAD^+. Fluorescent measurements (300 nm excitation/410 nm emission) of each well were taken in kinetic mode every 1 min for a total of 60 min in a Synergy H1 plate reader (BioTek). Initial rates were calculated based on linear fits of the first 3 min of the reaction.

Please cite this article in press as: Tal et al., Cyclic CMP and cyclic UMP mediate bacterial immunity against phages, Cell (2021), https://doi.org/10.1016/j.cell.2021.09.031

Negative stain electron microscopy and processing

50 μM (~1.66 mg mL^{-1}) *Bc*PycTIR was incubated with an equimolar ratio of cyclic nucleotide in gel filtration buffer (20 mM HEPES-KOH pH 7.5, 150 mM KCl, 1 mM TCEP) on ice for ~5 min. Mixtures were then serially diluted to a final concentration of 0.15 mg mL^{-1} protein with gel filtration buffer supplemented with the appropriate cyclic nucleotide at 50 μM. 3 μL of each sample were applied to a glow-discharged (30 s, 30 mA) 400-mesh carbon-coated grid, followed by a 30 s absorption step and side blotting to remove bulk solution. The grid was immediately stained twice with a 1.5% uranyl formate solution, with side blotting after each step.

Electron micrographs (30 micrographs for each condition) were collected using an FEI Tecnai T12 TEM operated at 120 keV equipped with a Gatan 4K × 4K CCD camera at a nominal magnification of 67,000 × , corresponding to a calibrated pixel size of 1.68 Å, and a target defocus of −1.5 μm. Image processing was performed in RELION-3.1 (Zivanov et al., 2020). CTF estimation was performed with CTFFIND4.1 (Rohou and Grigorieff, 2015). Particles were either picked manually or using Gautomatch (Kai Zhang; https://www.mrc-lmb.cam.ac.uk/kzhang/) followed by manual curation. Particles were extracted using a 148 pixel box size and subjected to 2D reference-free classification using a circular 225 Å diameter mask.

Pb8 binding assay

An *in vitro* pull-down experiment was designed to assess the ability of purified phage T5 pb8 protein to form a stable interaction with *Ec*PycC. An N-terminal 6 × His-SUMO2-tagged construct of pb8 was purified as described above for the cyclases and *Bc*PycTIR. 0.5 μM *Ec*PycC 'bait' protein which contained an N-terminal 6 × His-MBP-SUMO2 tag was incubated (30 min, 4°C) with 100 μL of 50% slurry (50 μL packed beads) amylose resin (New England Biolabs) diluted in 400 μL of binding buffer (20 mM HEPES-KOH pH 7.5, 100 mM KCl, 1 mM TCEP, 0.01% NP-40 detergent). 4 μM (8 × ['bait']) untagged pb8 protein ('prey') was added to the mixture and incubated for an additional 1 h at 4°C. Resin was pelleted at 4°C and 500 × g for 3 min and the supernatant was removed by aspiration. The beads were washed, pelleted, and resuspended in 1 mL of binding buffer a total of 4 times before 'elution' was achieved by heating the beads at 95°C for 2 min in 50 μL of SDS-PAGE loading dye. Eluted samples were loaded onto a 10% SDS-PAGE gel and visualized with Coomassie staining.

QUANTIFICATION AND STATISTICAL ANALYSIS

The average of triplicates is shown throughout with individual points overlaid, unless stated otherwise

Supplemental figures

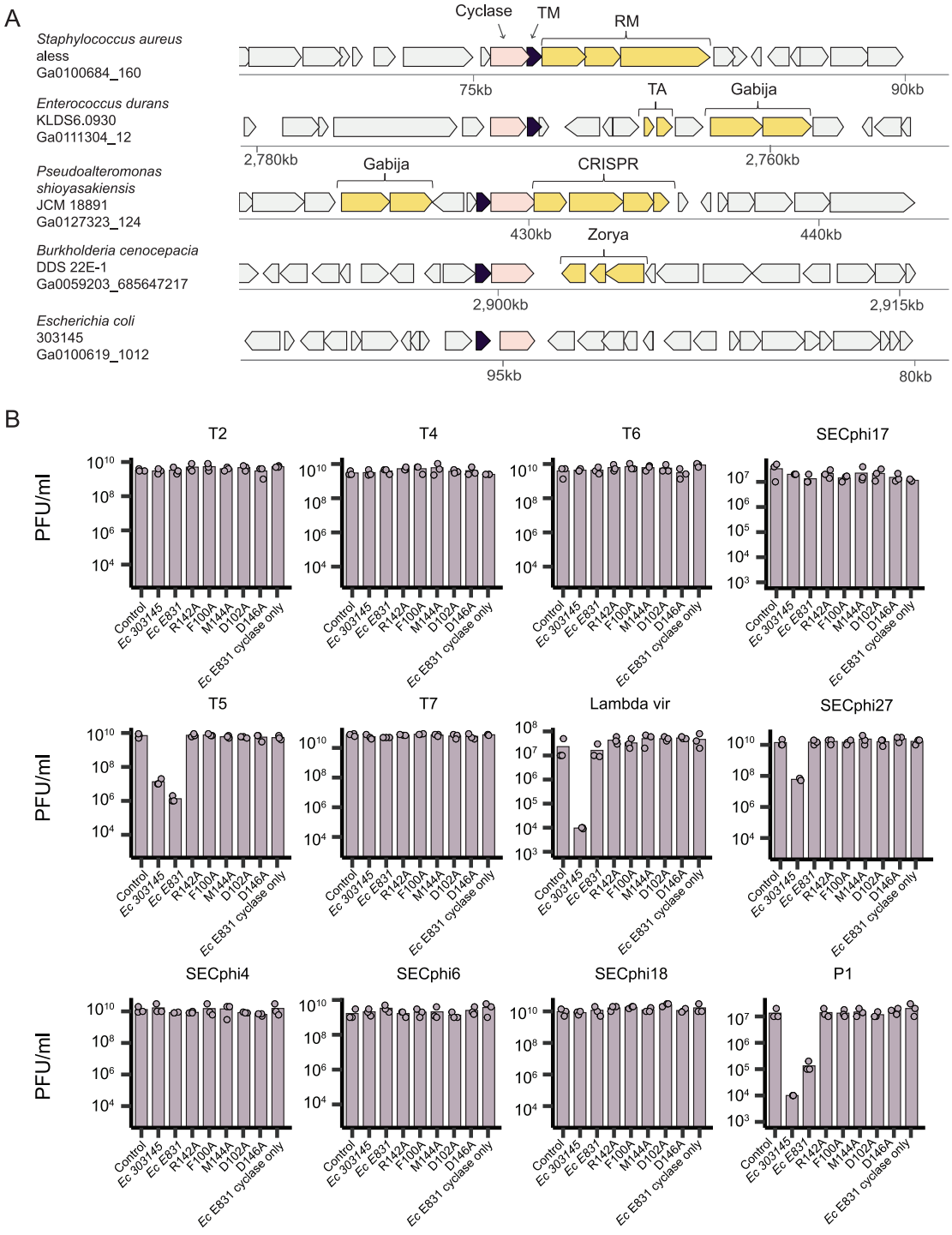

Figure S1. A two-gene defense system found in defense islands, related to Figures 1A and 1B

(A) Representative instances of a two-gene system encoding a gene with nucleotide cyclase domain (pink) and a gene with transmembrane (TM) domains (purple), in their genomic neighborhoods. Genes known to be involved in defense are shown in yellow. RM, restriction modification; Gabija and Zorya are a recently described defense systems (Doron et al., 2018). The bacterial species and the accession of the relevant genomic scaffold in the Integrated Microbial

(legend continued on next page)

Genomes (IMG) database (Chen et al., 2019) are indicated on the left. (B) Bacteria expressing WT Pycsar systems from *E. coli* 303145 or *E. coli* E831, as well as the system from *E. coli* E831 with point mutations in the cyclase or deletion of the TM effector ("cyclase only"), and a negative control that contains an empty vector, were grown on agar plates in room temperature. Tenfold serial dilutions of the phage lysate were dropped on the plates. Data represent plaque-forming units per milliliter for phages tested in this study. Each bar graph represents average of three replicates, with individual data points overlaid. The data for T5-infected WT and mutated *E. coli* E831 Pycsar are also presented in Figures 1C and 3F.

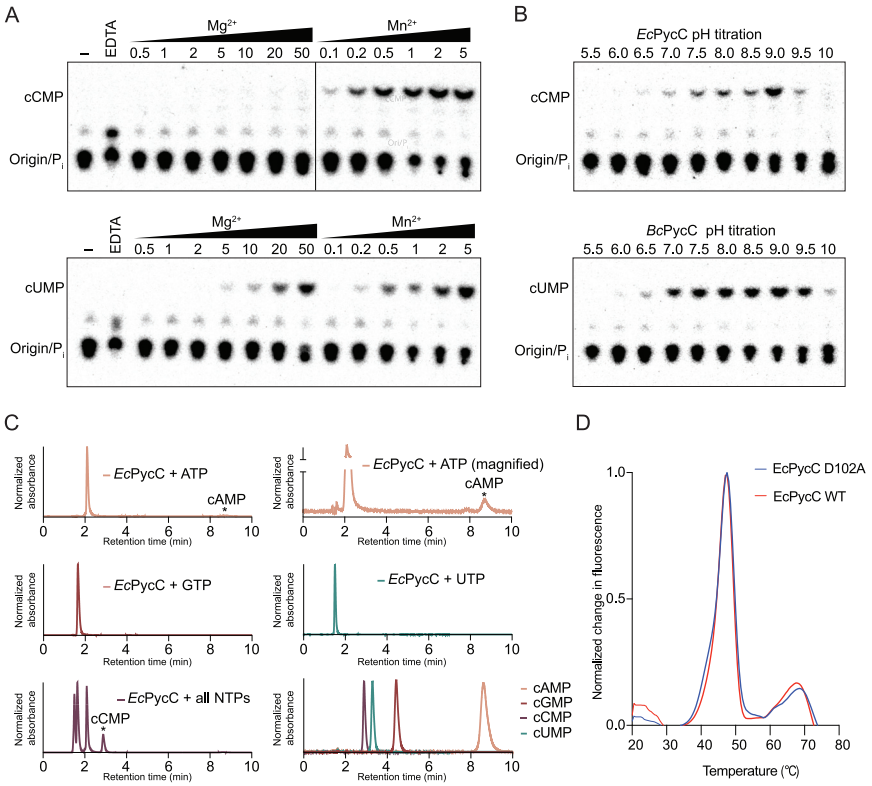

Figure S2. *In vitro* characterization of *Ec*PycC and *Bc*PycC cyclase catalytic activities, related to Figures 1D, 1E, and 2C

(A) Titration of divalent cation concentrations affects the *in vitro* activity of the *Ec*PycC (top) and *Bc*PycC (bottom) cyclases. Magnesium and manganese concentrations are in mM. (B) Cyclases display optimal activity at a broad range of neutral to basic pH. (C) HPLC traces for *Ec*PycC *in vitro* reactions with individual NTPs showing no significant cyclase activity for non-cognate substrates. Chemical standards were used to confirm reaction products. (D) Thermofluor stability assays of WT and mutant *Ec*PycC. Assays were performed in the following conditions: 3 × SYPRO orange fluorescent dye, 20 μM enzyme, 20 mM HEPES pH 7.5, 100 mM KCl buffer. 20 μL reaction volume. Measured at 20–95°C at 0.5°C increments every 30 s. Average of three independent experiments is shown.

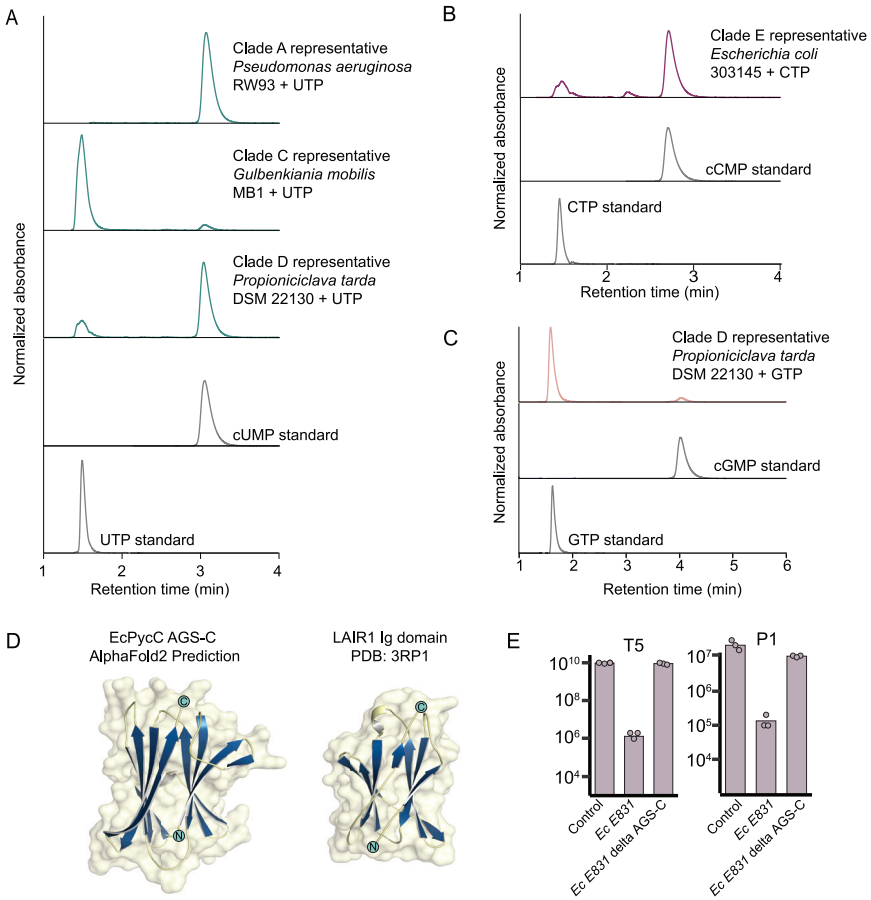

Figure S3. Biochemical analysis of cyclic pyrimidine mononucleotide phosphate synthases, related to Figure 2

(A) HPLC separation of primary cyclic nucleotide products generated by representative uridylate cyclases from various clades of the PycC phylogeny. (B) HPLC analysis displaying cCMP synthesis activity for an additional clade E cyclase. (C) Some synthases can produce minor quantities of cGMP *in vitro*. All reactions contained 500 μM NTPs and 5 μM enzyme. For panels A through C, HPLC of standard molecule is shown in gray. (D) The AGS-C domain of *Ec*PycC (residues 318–450) shares predicted structural homology to immunoglobulin fold protein domains. Prediction was carried out with AlphaFold2 Google collaborative notebook with default parameters (Jumper et al., 2021). (E) Bacteria expressing the WT Pycsar system from *E. coli* E831, the same system with *Ec*PycC in which the AGS-C domain was deleted, and a negative control that contains an empty vector, were grown on agar plates in room temperature. Tenfold serial dilutions of phage lysates (T5 and P1) were dropped on the plates. Data represent plaque-forming units per milliliter of the tested phages. Each bar graph represents average of three replicates, with individual data points overlaid.

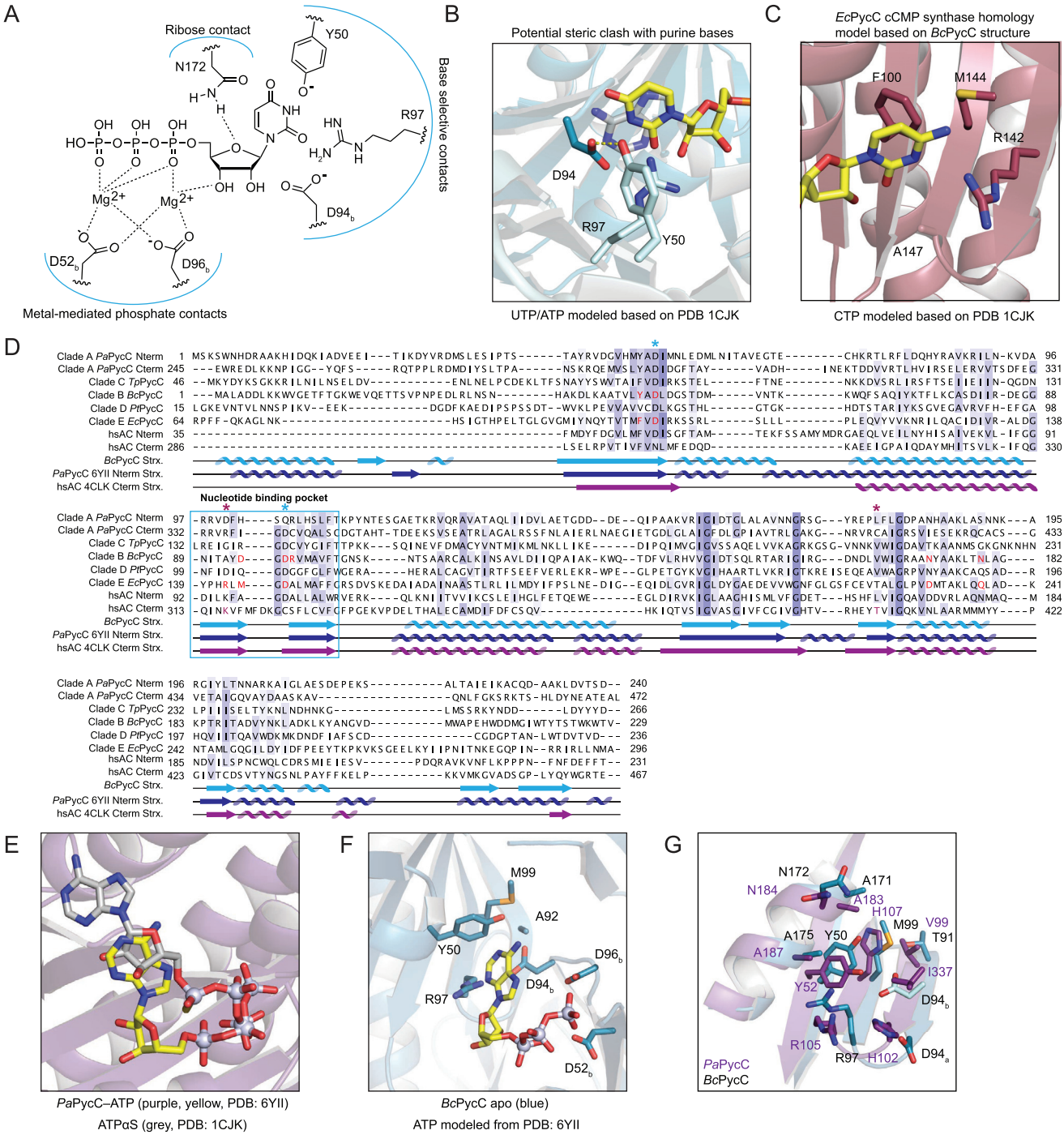

Figure S4. Sequence alignment and structural comparisons of PycC cyclases, related to Figure 3

(A) Representation of *Bc*PycC UTP binding pocket highlighting proposed amino acid contacts. A "b" subscript indicates residue contacts from the opposing monomer in the dimeric active site. (B) ATPαS modeled (transparent gray) into the *Bc*PycC binding pocket would cause significant clashing interactions with active site residues. UTP (yellow) modeled based on alignment with ATPαS in 1CJK (C) Homology model of the CTP binding pocket in *Ec*PycC prepared with the Phyre2 prediction server (Kelley et al., 2015) using the crystal structure of *Bc*PycC cUMP synthase as a template and CTP (yellow) modeled based on alignment with ATPαS in 1CJK. (D) Structure guided sequence alignment of nucleotide cyclases. Structure of *Bc*PycC of clade B was used to seed sequence alignment with Promals3D. For the two-domain cyclases *Pa*PycC of clade A and human soluble adenylate cyclase, both N- and C-term cyclase domains are depicted. Blue asterisks indicate catalytic residues. Purple asterisks indicate residues known to be important for selection of adenosine base in most adenylate cyclases. Residues in red were mutated in this study. Purple shading depicts sequence conservation. (E) *Pa*PycC (PDB: 6YII) binds ATP (yellow) in a configuration that differs significantly from the extended ATPαS binding configuration in 1CJK (gray), and is not compatible for cyclization. (F) The non-productive ATP conformation

(legend continued on next page)

observed in the *Pa*PycC structure can be potentially accommodated in the *Bc*PycC binding pocket but notably in both *Pa*PycC and *Bc*PycC active sites steric clashes would prevent the extended and cyclization competent configuration. (G) Superposition of *Pa*PycC and *Bc*PycC nucleotide binding pockets (ATP removed for clarity).

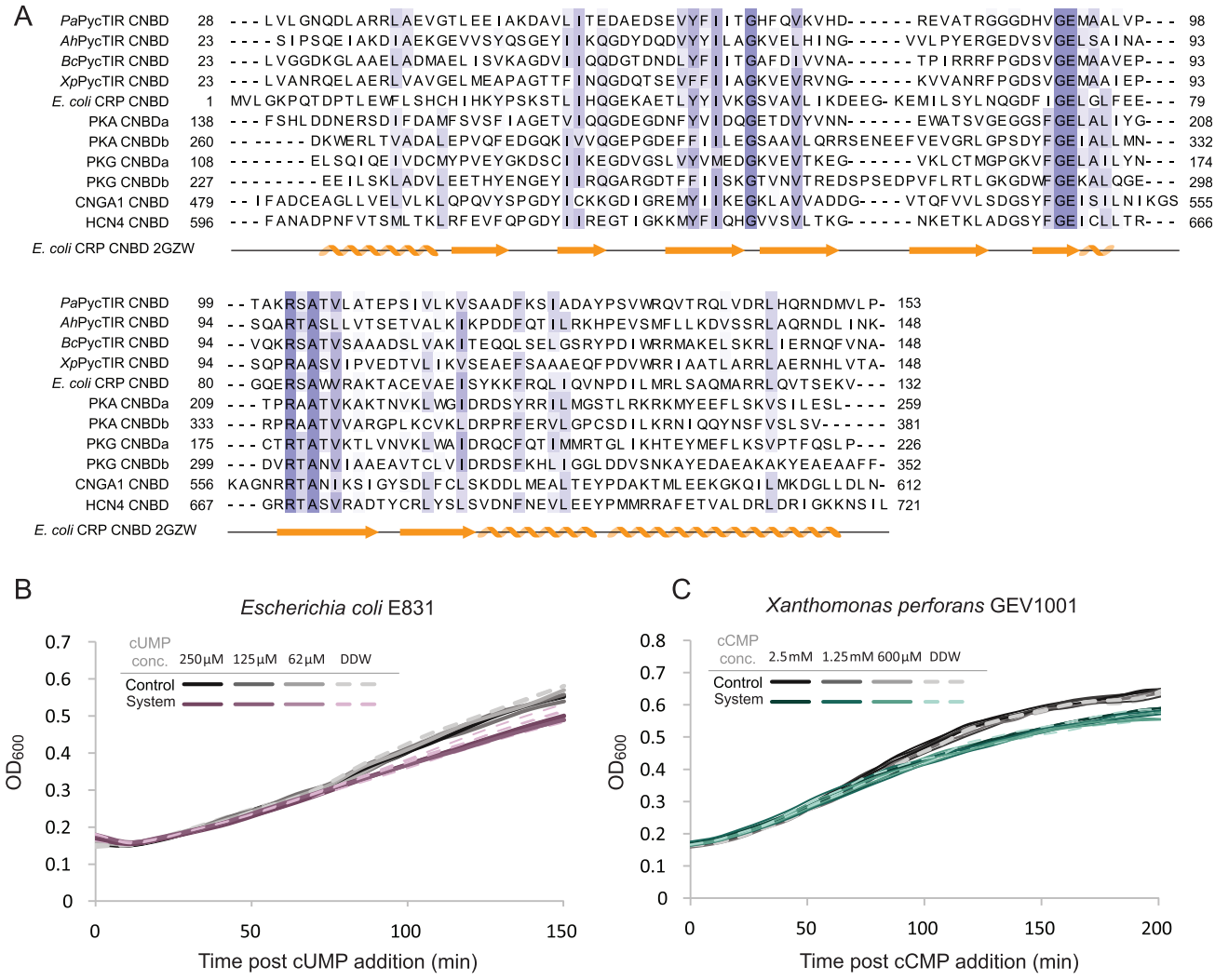

Figure S5. Pycsar effector specificity to cyclic nucleotides, related to Figures 4B and 5B

(A) Sequence alignment of cyclic nucleotide binding domains (CNBD, pfam: PF00027) of PycTIR proteins and previously studied CNBDs. Sequences were aligned using MAFFT and Promals3D. Presented are CNBDs from *Pa*PycTIR, *Ah*PycTIR, *Bc*PycTIR and *Xp*PycTIR, *E. coli* cAMP receptor protein (CRP), *H. sapiens* PRKAR1α cAMP-dependent protein kinase type I-α regulatory subunit (PKA), *H. sapiens* PRKG1 cGMP-dependent protein kinase 1 (PKG), *H. sapiens* cGMP-gated cation channel alpha-1 (CNGA1), and *H. sapiens* hyperpolarization-activated cyclic nucleotide-gated channel 4 (HCN4). (B-C) Non-cognate cyclic nucleotides are not toxic to Pycsar-expressing cells. (B) Growth curves of *E. coli* MG1655 cells expressing the Pycsar system from *E. coli* E831 (purple) and control cells (black) with and without the addition of the non-cognate ligand cUMP to the medium at various concentrations. (C) Growth curves of *E. coli* MG1655 cells expressing the Pycsar system from *X. perforans* GEV1001 (blue) and control cells (black) with and without the addition of the non-cognate ligand cCMP to the medium at various concentrations. For both panels B and C, results of three experiments are presented as individual curves.

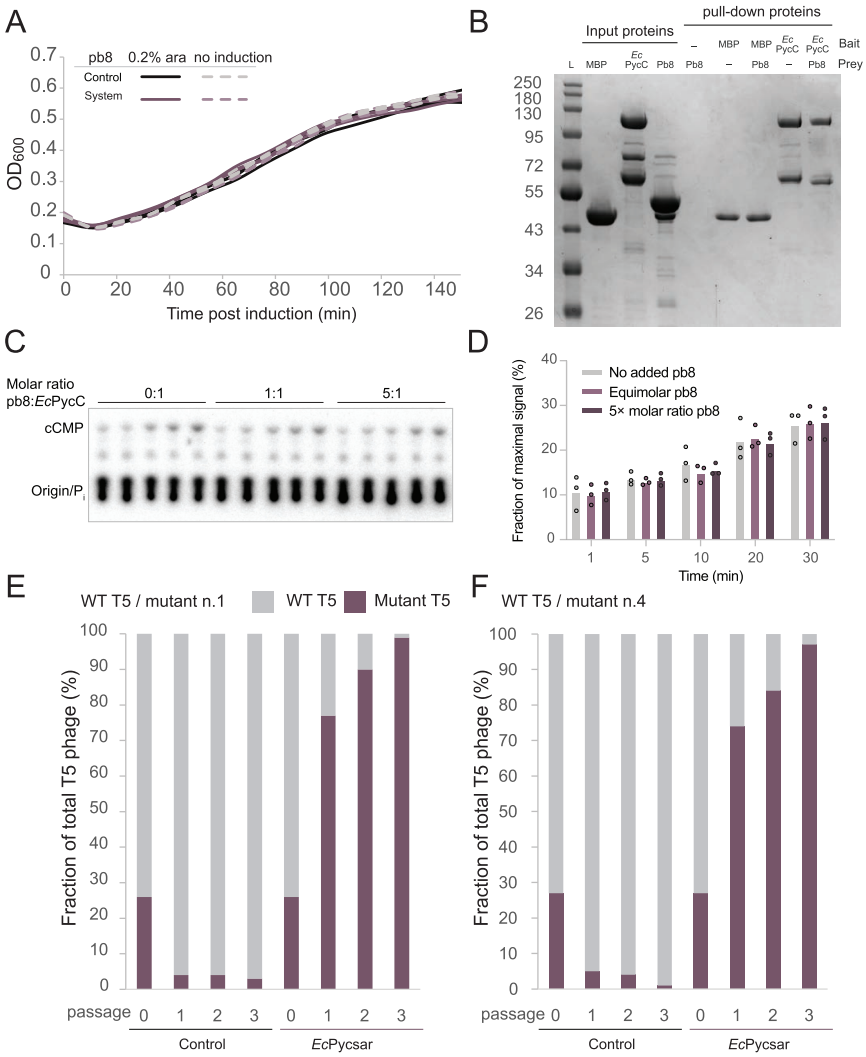

Figure S6. Phages mutated in the Pb8 protein, related to Figure 6

(A) Growth curves of *E. coli* MG1655 cells expressing the Pycsar system from *E. coli* E831, that also contain a vector harboring the pb8 protein under an inducible promoter (purple) and control cells (black) containing the same pb8-containing construct but not the defense system. Results of three experiments are presented as individual curves. x axis represents minutes post arabinose induction. (B) *In vitro* pull-down assay using MBP-tagged proteins demonstrating lack of interaction between T5 pb8 and the *E. coli* E831 PycC cyclase. *Ec*PycC was expressed with an N-terminal 6 × His–MBP–SUMO2 tag and the resulting full-length protein has a predicted molecular weight of ~105 kDa. The lower molecular weight bands correspond to truncated 6 × His–MBP species co-purified during Ni-NTA purification. (C,D) The impact of pb8 T5 phage capsid protein on cyclase activity of *Ec*PycC was assessed via thin-layer chromatography. Reactions contained 1 μM *Ec*PycC and 0, 1, or 5 μM purified pb8 in buffer containing 50 mM Tris pH 8.5, 1 mM $MnCl_2$, 100 mM KCl, 500 μM CTP, and trace α-^{32}P-CTP. Reactions were incubated for the indicated times at 37°C, quenched at 85°C for 2 min, cooled on ice for 2 min, then treated with CIP for 30 min at 37°C to digest uncyclized CTP. (C) A representative TLC image. (D) The percent fractional signal associated with cCMP production from three independent experiments was quantified and average values are plotted, with individual data points overlaid. (E,F) A competition fitness assay between WT and mutant T5 phages (mutant n.1 and mutant n.4 for panels C and D, respectively) on both Pycsar-expressing and control cells. y axis represents the fraction of each strain out of the total phage mixture based on sequenced DNA reads. x axis represents the infection passage, with 0 representing the mixture prior to first passage. In each passage, phage lysate was taken and used for infection of a fresh bacterial culture.